ERDC/EL TR-08-37

Environmental Laboratory

US Army Corps
of Engineers®
Engineer Research and
Development Center

Environmental Quality and Installations Program

UXO Characterization: Comparing Cued Surveying to Standard Detection and Discrimination Approaches

Report 6 of 9
Advanced Electromagnetic and Magnetic Methods for Discrimination of Unexploded Ordnance

Stephen D. Billings, Leonard R. Pasion, Nicolas Lhomme and Lin Ping Song

September 2008

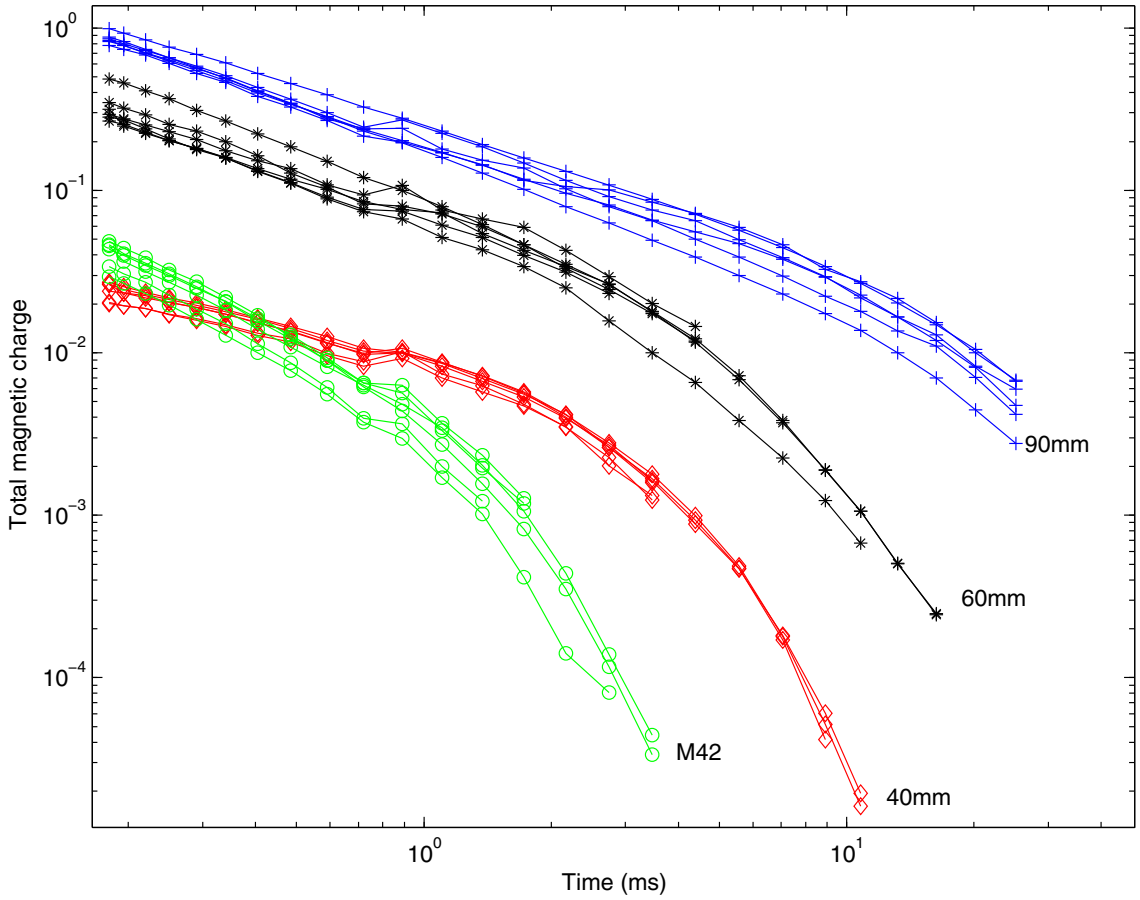

Environmental Quality and Installations Program

ERDC/EL TR-08-37
September 2008

UXO Characterization: Comparing Cued Surveying to Standard Detection and Discrimination Approaches

Report 6 of 9
Advanced Electromagnetic and Magnetic Methods for Discrimination of Unexploded Ordnance

Stephen D. Billings and Leonard R. Pasion

Sky Research, Inc.
445 Dead Indian Memorial Rd.
Ashland, OR 97520-9706

Nicolas Lhomme and Lin Ping Song

Earth and Ocean Science Department
University of British Columbia
Vancouver, B.C., Canada, V6T 1Z4

Report 6 of 9

Prepared for Headquarters, U.S. Army Corps of Engineers
Washington, DC 20314-1000

Monitored by Environmental Laboratory
U.S. Army Engineer Research and Development Center
3909 Halls Ferry Road, Vicksburg, MS 39180-6199

Abstract: The magnetic and electromagnetic induction models and inversion strategies that are used to discriminate hazardous UXO from non-hazardous shrapnel and scrap metal are described. Discrimination methods typically proceed by first recovering a set of parameters that specify a physics-based model of the object being interrogated. For EMI, a polarizability model is commonly used. For magnetics, the physics-based model is generally a static magnetic dipole. Once the parameters are recovered by inversion, a subset of the parameters is used as feature vectors to guide a statistical or rule-based classifier. The dipole-based inversion and classification scheme is described and a number of variations are considered, including: 1) Dipole-based template matching whereby the object's identity is selected as the best fitting polarization model from a predefined library of objects; 2) SEA, where the dipole model is replaced with a physically complete forward-modeling scheme. SEA is also a template-matching approach; and 3) SMC, where the dipole model is replaced by a fictitious charge distribution on a circle or ellipse that encloses the UXO or clutter object. The total SMC is then used as a feature vector in a statistical or rule-based classification scheme.

Contents

Figures and Tables

Figures

Table

Preface

This report was prepared as part of the Congressional Interest Environmental Quality and Installations Program, Unexploded Ordnance (UXO) Focus Area, Contract No. W912HZ-04-C-0039, Purchase Request No. W81EWF-418-0425, titled, "UXO Characterization: Comparison of Cued-Surveying to Standard Detection and Standard Discrimination Approaches." Research was conducted by Sky Research, Inc., for the Environmental Laboratory (EL), U.S. Army Engineer Research and Development Center (ERDC), Vicksburg, MS. The following Sky Research personnel contributed to this report:

- Dr. Stephen D. Billings was the project PI and oversaw the research presented in this report.
- Dr. Leonard R. Pasion developed the fingerprinting method and assisted with the development of the Surface Magnetic Charge (SMC) and Standardized Excitations Approach (SEA) methods.
- Joy Rogalla was the copy editor for this report.

The following personnel from the University of British Columbia contributed to this report:

- Dr. Nicolas Lhomme developed the SMC methodology.
- Dr. Lin Ping Song developed the SEA methodology.

Dr. Fridon Shubitidze from Dartmouth College originally developed the SMC and SEA methods and contributed to the developments presented herein.

The theoretical development of the Standardized Excitations Approach and the Surface Magnetic Charge method were supported under SERDP-UX-1446: "A Unified Approach to UXO Discrimination Using the Method of Auxiliary Sources." The initial development work for these methods was conducted by Dr. Shubitidze and Dr. Kevin O'Neill, Cold Regions Research and Engineering Laboratory, ERDC.

This project was performed under the general supervision of Dr. M. John Cullinane, Jr., Technical Director, Military Environmental Engineering and Sciences, EL, and John H. Ballard, Office of Technical Director and UXO Focus Area Manager, EL. Reviews were provided by Ballard and Dr. Dwain Butler, Alion Science and Technology Corporation.
Dr. Elizabeth Fleming was Director, EL.

COL Gary E. Johnston was Commander and Executive Director of ERDC.
Dr. James R. Houston was Director.

Acronyms

2D	Two-dimensional
3D	Three-dimensional
ATC	Aberdeen Test Center
BOR	Body of Revolution
cm	centimeter(s)
DoD	Department of Defense
DSB	Defense Science Board
EM	Electromagnetic
EMI	Electromagnetic Induction
ERDC	Engineer Research and Development Center
ESTCP	Environmental Security Technology Certification Program
FEM	Frequency Domain Electromagnetics
GLRT	Generalized Likelihood Ratio Test
H/m	Henry per meter
IMU	Inertial Motion Unit
m	meter(s)
MAS	Method of Auxiliary Sources
mm	millimeter(s)
ms	millisecond(s)
NSMC	Normalized Surface Magnetic Charge
nT	nanoTesla
PNN	Probabilistic Neural Network
P-O	Pasion-Oldenburg
ROC	Receiver Operating Characteristic
RSS	Reduced Source Sets
SEA	Standardized Excitations Approach
SMC	Surface Magnetic Charge
SNR	Signal-to-Noise Ratio

SVM	Support Vector Machine
TEM	Time Domain Electromagnetic
TMC	Total Magnetic Charge
TNMC	Total Normalized Magnetic Charge
UBC	University of British Columbia
UBC-GIF	University of British Columbia – Geophysical Inversion Facility
UTM	Universal Transverse Mercator
UXO	Unexploded Ordnance
USACE	U.S. Army Corps of Engineers

General Information

The clearance of military facilities in the United States contaminated with unexploded ordnance (UXO) is one of the most significant environmental concerns facing the Department of Defense. A 2003 report by the Defense Science Board (DSB) on the topic estimated costs of remediation in the tens of billions of dollars. The DSB recognized that development of effective discrimination strategies to distinguish UXO from non-hazardous material is one essential technology area where the greatest cost saving to the Department of Defense (DoD) can be achieved.

The objective of project W912HZ-04-C-0039 "UXO Characterization: Comparison of Cued-Surveying to Standard Detection and Standard Discrimination Approaches," was to research, develop, optimize, and evaluate the efficiencies of different modes of UXO characterization and remediation as a function of the density of UXO and associated clutter. Survey modes investigated in the research include:

1. Standard detection survey: All selected anomalies are excavated;
2. Advanced discrimination survey: Data collected in proximity to each identified anomaly are inverted for physics-based parameters and statistical or analytical classifiers are used to rank anomalies, from which a portion of the higher ranked anomalies are excavated;
3. Cued survey mode: Each selected anomaly is revisited with an interrogation platform, high-quality data are collected and analyzed, and a decision is made as to whether to excavate the item, or leave it in the ground.

Specific technical objectives of the research were to:

- Determine the feasibility and effectiveness of various interrogation approaches based on the cued survey approach;
- Determine the feasibility and effectiveness of various interrogation sensors including magnetics, ground penetrating radar (GPR), and electromagnetic (EM) induction (EMI), and evaluate combinations of these sensors;
- Develop and evaluate the most promising interrogation platform designs;

- Develop optimal processing and inversion approaches for cued-interrogation platform datasets;
- Evaluate the data requirements to execute accurate target parameterization and assess the technical issues of meeting these requirements using detection and interrogation survey techniques;
- Determine which survey mode is most effective as a function of geological interference, and UXO/clutter density;
- Investigate the feasibility and effectiveness of using detailed test-stand measurements on UXO and clutter to assist in the design of interrogation algorithms used in the cued-search mode.

The main areas of research involved in these coordinated activities include:

- Sensor phenomenology including GPR, EMI , and magnetometry;
- Data Collection Systems; platforms, field survey systems, field interrogation systems;
- Parameter estimation techniques; inversion techniques (single, cooperative, joint), forward-model parameterizations, processing strategies; and
- Classification methods; thresholding, statistical models, information systems.

This report "UXO Characterization: Comparing Cued Surveying to Standard Detection and Discrimination Approaches: Report 6 of 9 – Advanced Electromagnetic and Magnetic Methods for Discrimination of Unexploded Ordnance" is one of a series of nine reports written as part of W912HZ-04-C-0039:

1. UXO Characterization: Comparing Cued Surveying to Standard Detection and Discrimination Approaches: Report 1 of 9 – Summary Report;
2. UXO Characterization: Comparing Cued Surveying to Standard Detection and Discrimination Approaches: Report 2 of 9 – Ground Penetrating Radar for Unexploded Ordnance Characterization; Fundamentals;
3. UXO Characterization: Comparing Cued Surveying to Standard Detection and Discrimination Approaches: Report 3 of 9 – Test Stand Magnetic and Electromagnetic Measurements of Unexploded Ordnance;

4. UXO Characterization: Comparing Cued Surveying to Standard Detection and Discrimination Approaches: Report 4 of 9 – UXO Characterization Using Magnetic, Electromagnetic, and Ground Penetrating Radar Measurements at the Sky Research Test Plot;
5. UXO Characterization: Comparing Cued Surveying to Standard Detection and Discrimination Approaches: Report 5 of 9 – Optimized Data Collection Platforms and Deployment Modes for Unexploded Ordnance Characterization;
6. UXO Characterization: Comparing Cued Surveying to Standard Detection and Discrimination Approaches: Report 6 of 9 – Advanced Electromagnetic and Magnetic Methods for Discrimination of Unexploded Ordnance;
7. UXO Characterization: Comparing Cued Surveying to Standard Detection and Discrimination Approaches: Report 7 of 9 – Marine Corps Base Camp Lejeune: UXO Characterization Using Ground Penetrating Radar;
8. UXO Characterization: Comparing Cued Surveying to Standard Detection and Discrimination Approaches: Report 8 of 9 – Marine Corps Base Camp Lejeune: UXO Characterization Using Magnetic and Electromagnetic Data;
9. UXO Characterization: Comparing Cued Surveying to Standard Detection and Discrimination Approaches: Report 9 of 9 – Former Lowry Bombing and Gunnery Range: Comparison of UXO Characterization Performance Using Area and Cued-interrogation Survey Modes.

1 Introduction

Magnetic and electromagnetic (EM) methods represent the primary sensor types used for detection of UXO. Over the past 10 years, significant research effort has been focused on developing methods to discriminate between hazardous UXO and non-hazardous scrap metal, shrapnel, and geology (e.g., Hart et al. 2001; Collins et al. 2001; Pasion and Oldenburg 2001a, 2001b; Zhang et al. 2003a, 2003b; Billings 2004). The most promising discrimination methods typically proceed by first recovering a set of parameters that specify a physics-based model of the object being interrogated. For example, in time-domain electromagnetic (TEM) data, the parameters comprise the object location and the polarization tensor (typically two or three collocated orthogonal dipoles along with their orientation and some parameterization of the time-decay curve). For magnetics, the physics-based model is generally a static magnetic dipole. Once the parameters are recovered by inversion, a subset of the parameters is used as feature vectors to guide either a statistical or rule-based classifier.

Magnetic and EM phenomenologies have different strengths and weaknesses. Magnetic data are simpler to collect, are mostly immune to sensor orientation and are better able to detect deeper targets. EM data are sensitive to non-ferrous metals, are better at detecting smaller items, and are able to be used in areas with magnetic geology. There are significant advantages in collecting both types of data, including increased detection, stabilization of the EM inversions by cooperative inversion of the magnetics (Pasion et al., in preparation) and extra dimensionality in the feature space that may improve classification performance (e.g., Zhang et al. 2003a). However, these advantages need to be weighed against the extra costs of collecting both data types.

Three key elements impact the success of the UXO discrimination process described in the previous paragraphs:

1. Creation of a map of the geophysical sensor data: This includes all actions required to form an estimate of the geophysical quantity in question (magnetic field in nanoTesla [nT], amplitude of EMI response at a given

time-channel, etc.) at each of the visited locations. The estimated quantity is dependent on the following:

   a. Hardware, including the sensor type, deployment platform, position and orientation system, and the data acquisition system used to record and time-stamp the various sensors;
   b. Survey parameters such as line spacing, sampling rate, calibration procedures, etc.;
   c. Data processing such as merging of position/orientation information with sensor data, noise and background filtering applied;
   d. Background environment including geology, vegetation, topography, cultural features, etc.
   e. Depth and distribution of ordnance and clutter.

2. Anomaly selection and feature extraction: This includes the detection of anomalous regions and the subsequent extraction of a dipole (for magnetics) or polarization tensor (for TEM) model for each anomaly. Where magnetic and EMI data have both been collected, the magnetic data can be used as constraints for the EMI model via a cooperative inversion process.
3. Classification of anomalies: Given the feature vectors and training data over a portion of the site, the final step in the process is the creation of a ranked dig-list. Either statistical or rule-based classifiers are used to order anomalies from most- to least-likely UXO.

This report describes the above dipole-based inversion and classification scheme. A number of variations to the scheme presented above are also considered, including:

1. Dipole-based template matching, whereby the object identity is selected as the best fitting polarization model from a predefined library of objects;
2. Standardized Excitations Approach (SEA) where the dipole model is replaced with a physically complete forward modeling scheme. SEA is also a template-matching approach; and
3. Surface Magnetic Charge (SMC) method, where the dipole model is replaced by a fictitious charge distribution on a circle or ellipse that encloses the UXO or clutter item. The total SMC is then used as a feature vector in a statistical or rule-based classification scheme.

The advantage of the SEA and SMC methods is that, unlike the dipole model, they are able to reproduce the response of an object in both the near and far fields. However, the methods are not yet as mature as the

dipole model, and the work described herein must be considered preliminary. Neither method can currently be used for discrimination of live-site data. In contrast, all of the dipole-based methods described here have been implemented in the University of British Columbia's (UBC's) UXOLab software package and are currently undergoing testing and evaluation at a number of sites.

UXOLab is a Matlab-based software package developed over a six-year period at the UBC-Geophysical Inversion Facility (GIF), principally through funding by the US Army Corps of Engineers (USACE) Engineer Research and Development Center (ERDC) (DAAD19-00-1-0120). Over the past three years (as part of this project and others), Sky Research and UBC-GIF have considerably expanded the capabilities of the software.

All of the methods described in this report assume that there is one object in the field of view of the sensor. That is, the case of highly cluttered sites where the responses from multiple items overlap is not considered.

2 UXO Discrimination Using Dipole Models

The two key elements of dipole-based classification are (1) feature extraction (or equivalently the inversion of the dipole parameters); and (2) classification. This section of the report reviews the methods used for these two steps.

2.1. Feature extraction

2.1.1. Feature extraction: Electromagnetic induction

In the EMI method, a time-varying field illuminates a buried, conductive target. Currents induced in the target then produce a secondary field that is measured at the surface. EM data inversion involves using the secondary field generated by the target for recovery of the position, orientation, and parameters related to the target's material properties and shape. For UXO, the inverse problem is simplified by assuming that the secondary field can be accurately approximated as a dipole.

In order to illuminate a buried target, TEM sensors generate a large primary field that is rapidly switched off. The currents induced in the buried target decay with time, generating a decaying secondary field that is measured at the surface. The time-varying secondary magnetic field $\mathbf{B}(t)$ at a location $\mathbf{r}$ from the dipole $\mathbf{m}(t)$ is

$$\mathbf{B}(t) = \frac{\mu_o}{4\pi r^3}\mathbf{m}(t)\cdot\left(3\hat{\mathbf{r}}\hat{\mathbf{r}} - \mathbf{I}\right) \tag{1}$$

where $\hat{\mathbf{r}} = \mathbf{r} / |\mathbf{r}|$ is the unit-vector pointing from the dipole to the observation point, $\mathbf{I}$ is the 3×3 identity matrix, $\mu_0 = 4\pi \times 10^{-7}$ H/m is the permittivity of free space and $r = |\mathbf{r}|$ is the distance between the center of the object and the observation point. Equation 1 assumes an ideal step-off field and can be modified to account for arbitrary transmitter waveforms.

The dipole induced by the interaction of the primary field $\mathbf{B}_o$ and the buried target is given by

$$\mathbf{m}(t) = \frac{1}{\mu_o}\mathbf{M}(t)\cdot\mathbf{B}_o \tag{2}$$

where $\mathbf{M}(t)$ is the target's polarization tensor. The polarization tensor governs the decay characteristics of the buried target and is a function of the shape, size, and material properties of the target. The polarization tensor is written as:

$$\mathbf{M}(t) = \begin{bmatrix} L_1(t) & 0 & 0 \\ 0 & L_2(t) & 0 \\ 0 & 0 & L_3(t) \end{bmatrix} \tag{3}$$

using the convention that $L_1(t_1) \geq L_2(t_1) \geq L_3(t_1)$, so that polarization tensor parameters are organized from largest to smallest. The polarization tensor components are parameterized such that the target response can be written as a function of a model vector containing components that are a function of target characteristics. Particular parameterizations differ depending on the instrument (number of time channels, time range measured, etc.) and the group implementing the work. Bell et al. (2001) solve for the components of the polarization tensor at each time channel, and this procedure is used for the four-channel Geonics EM-61 MKII. The Geonics EM-63 uses the Pasion-Oldenburg (P-O) formulation (Pasion and Oldenburg 2001a, 2001b), with $\alpha_i = 0$,

$$L_i(t) = k_i \left(t + \alpha_i\right)^{-\beta_i} \exp\left(-t / \gamma_i\right) \tag{4}$$

for $I = \{1, 2, 3\}$ and with the convention that $k_1 \geq k_2 \geq k_3$. For a rod-like body of revolution (BOR), the axial polarization is the largest L_1, while the transverse polarizations are smaller and equal, $L_2 = L_3$ (Pasion and Oldenburg 2001a, 2001b). For a plate-like body of revolution, the transverse polarizations are equal, $L_1 = L_2$, and larger than the axial polarization.

The GEM-3 (frequency domain system) uses either the instantaneous polarization model or the four-parameter model of Miller et al. (2001),

$$L(\omega) = k\left(s + \frac{(i\omega\tau)^c - 2}{(i\omega\tau)^c + 1}\right) \tag{5}$$

where ω is angular frequency, k is the object amplitude, τ is a response time-constant, s is a factor that controls the magnitude of asymptotes at

high and low frequency, and c is a parameter that controls the width of the peak in the in-phase data.

Given a set of observations $\mathbf{d}^{\mathbf{obs}}$, the parameter estimation is formulated as an optimization problem through Bayes theorem:

$$p\left(\mathbf{m} \mid \mathbf{d}^{\mathbf{obs}}\right) = \frac{p(\mathbf{m})\, p\left(\mathbf{d}^{\mathbf{obs}} \mid \mathbf{m}\right)}{p\left(\mathbf{d}^{\mathbf{obs}}\right)} \tag{6}$$

where $\mathbf{m}$ is the vector of model parameters (location, orientation and polarization tensor parameters), $p(\mathbf{m})$ is the probability distribution representing prior information, $p(\mathbf{d}^{\mathbf{obs}})$ is the marginal probability density of the experimental data, and $p(\mathbf{d}^{\mathbf{obs}}|\mathbf{m})$ is the conditional probability density of the experimental data, which describes the ability of the model to reproduce the experimental data. The a-posteriori conditional probability density $p(\mathbf{m}|\mathbf{d}^{\mathbf{obs}})$ is the probability density ascribed to $\mathbf{m}$ after collecting the data. The a-posteriori conditional probability density encapsulates all available information on the model parameters, and the model that maximizes it is usually regarded as the solution to the inverse problem. A value of $\mathbf{m}$ is estimated that maximizes the log of the a-posteriori conditional probability density

$$m^* = \max_{\mathbf{m}} \left\{ \log\left[p\left(\mathbf{m} \mid \mathbf{d}^{\mathbf{obs}}\right)\right]\right\} \tag{7}$$

With a single data set and no prior information on the model parameters (except bound constraints on the model parameters), the inversion reduces to

$$\text{minimize } \varphi(\mathbf{m}) = \frac{1}{2}\left\| V_d^{-1/2}\left[\mathbf{d}^{\mathbf{obs}} - F(m)\right]\right\|^2, \textit{ subject to } m_i^L \le m_i \le m_i^U \tag{8}$$

where $F(\mathbf{m})$ is a vector comprising the forward modeled data at the sampled locations, m_i^L and m_i^U are the lower and upper bounds on parameter i and V_d is the co-variance matrix of the data. Efficient algorithms for the solution of this optimization problem have been implemented for various polarization tensor formulations within UXOLab (including two and three independent component polarization tensors).

The accuracy of the feature vectors recovered by inversion depends on the signal-to-noise ratio, position and orientation accuracy of the sensor data, and spatial coverage of the available data. As described in Appendix A, accurately resolving both the transverse and axial polarizations of a buried object can be challenging when using horizontal transmitter loops (such as the Geonics EM-61 and EM-63 and Geophex GEM-3 data used in this project). Successful discrimination requires careful attention to factors that affect data quality (see Report 5 in this series for examples of platforms and data collection procedures developed as part of this project).

2.1.2. Feature extraction: Magnetics

For magnetics, the physics-based model most commonly used is a dipole. This comprises a location (horizontal position and depth) and the magnitude and orientation of the dipole moment. More complicated models comprising quadrupoles and octupoles have been developed (Billings et al. 2002a, 2002b). However, in most UXO detection scenarios the sensor is in the far field of the source body and moments of higher order than the dipole are poorly resolved. The contribution of the dipole to the magnetic field decays as the third power of distance from the object and dominates the far field,

$$\mathbf{B}(\mathbf{r}) = \frac{\mu_o}{4\pi r^3}\mathbf{m}\cdot\left(3\hat{\mathbf{r}}\hat{\mathbf{r}} - \bar{\bar{\mathbf{I}}}\right) \tag{9}$$

where the terms were defined earlier. As for the TEM case, a bound-constrained optimization problem is solved to extract feature vectors from each anomaly.

2.2. Classification of anomalies

At this stage in the process, feature vectors have been established for each anomaly and a decision must be made as to which items should be excavated as potential UXO. Rule-based classifiers use relationships derived from the underlying physics to partition the feature space. Examples include the ratio of TEM decay parameters (Pasion and Oldenburg 2001a, 2001b) and magnetic remanence (Billings 2004). This project focuses on statistical classification techniques that have proven to be very effective at discrimination at various test sites (e.g., Zhang et al. 2004; Beran et al. 2004).

Statistical classifiers have been applied to a wide variety of pattern recognition problems, including optical character recognition, bioinformatics, and UXO discrimination. Within this field there is an important dichotomy between *supervised* and *unsupervised* classification. Supervised classification makes classification decisions for a *test* set comprised of unlabelled feature vectors. The classifier performance is optimized using a *training* data set for which labels are known. In unsupervised classification there is only a test set; labels are unknown for all feature vectors. Most applications of statistical classification algorithms to UXO discrimination have used supervised classification; the training data set is generated as targets are excavated. More recently, unsupervised methods have been used to generate a training data set which is an informative sample of the test data (Zhang et al. 2004). In addition, semi-supervised classifiers, which exploit both labeled data and the topology of unlabelled data, have been applied to UXO discrimination in one study (Zhang et al. 2004).

Figure 1 summarizes the supervised classification process within the statistical framework. Given test and training data sets, features can be extracted from the data, a relevant subset of these features can be selected, and the classifier can be optimized using the available training data. Because the predicted performance of the classifier is dependent upon the feature space, the learning stage can involve further experimentation with feature extraction and selection before adequate performance is achieved.

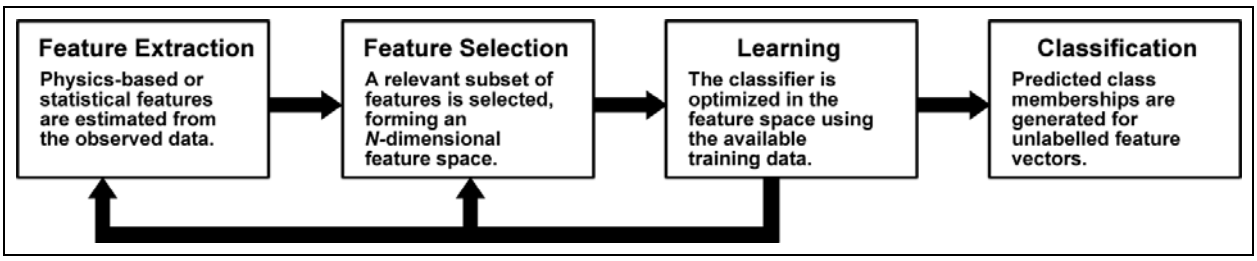

Figure 1. A framework for statistical pattern recognition.

There are two (sometimes equivalent) approaches to partitioning the feature space. The *generative* approach models the underlying probability distributions, which are assumed to have produced the observed feature data. The starting point for any generative classifier is Bayes rule:

$$\mathrm{P}\left(\omega_i \middle| \mathbf{x}\right) \propto \mathrm{P}\left(\mathbf{x} \middle| \omega_i\right)\mathrm{P}\left(\omega_i\right) \tag{10}$$

The likelihood function $P(\mathbf{x}|\omega_i)$ computes the probability of observing the feature vector **x** given the class ω_i. The prior probability $P(\omega_i)$ quantifies the expectation of how likely it is to observe class ω_i. Bayes rule provides a mechanism for classifying test feature vectors: assign **x** to the class with the largest *a posteriori* probability. Contours along which the posterior probabilities are equal define decision boundaries in the feature space.

An example of a generative classifier is discriminant analysis, which assumes a Gaussian form for the likelihood function. Training this classifier involves estimating the means and covariances of each class. If equal covariances are assumed for all classes, the decision boundary is linear. While these assumptions may seem overly restrictive, in practice linear discriminant analysis performs quite well in comparison with more exotic methods and is often used as a baseline classifier when assessing performance.

Other generative classifiers assume a nonparametric form for the likelihood function. For example, the probabilistic neural network (PNN) models the likelihood for each class as a superposition of kernel functions. The kernels are centered at the training data for each class. In this case the complexity of the likelihood function (and hence the decision boundary) is governed by the width of the kernels (Figure 2).

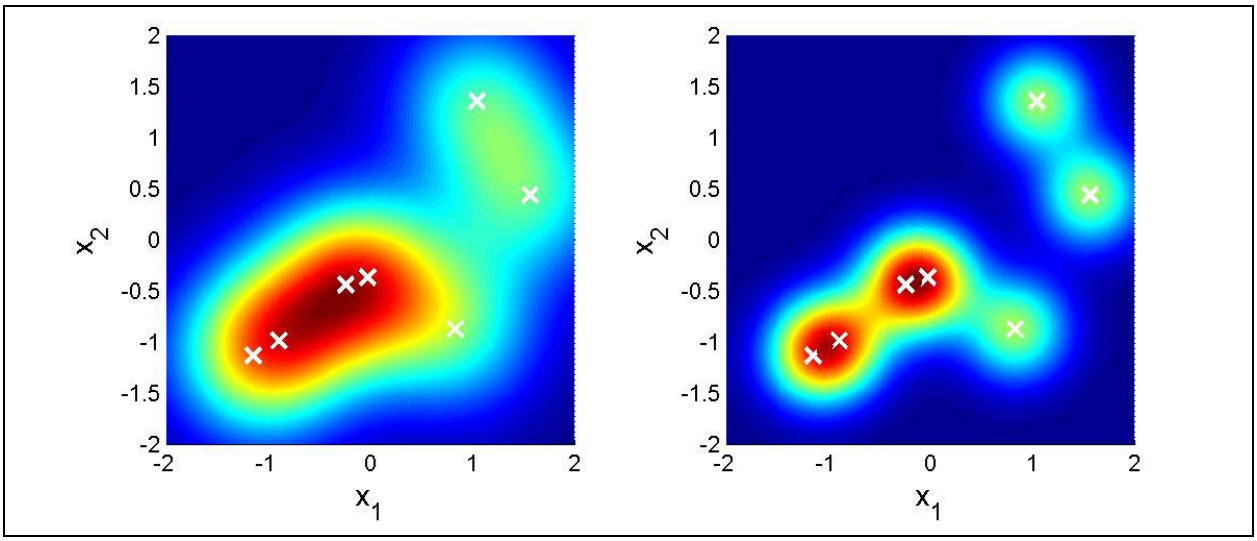

Figure 2. Nonparametric density estimate using Gaussian kernels. Kernel centers are shown as crosses. A large kernel width produces a smooth distribution (left) compared to a small kernel width (right).

The *discriminative* approach is not concerned with underlying distributions but rather seeks to identify decision boundaries, which provide an optimal separation of classes. For example, a support vector machine (SVM) constructs a decision boundary by maximizing the *margin* between classes. The margin is defined as the perpendicular distance between *support planes* which bound the classes, as shown in Figure 3. The decision boundary then bisects the support planes (the boundary does not have to be linear as shown in the example). This formulation leads to a constrained optimization problem: maximize the margin between classes subject to the constraint that the training data are classified correctly. An advantage of the SVM method over other discriminative classifiers (e.g., neural networks) is that there is a unique solution to the optimization problem.

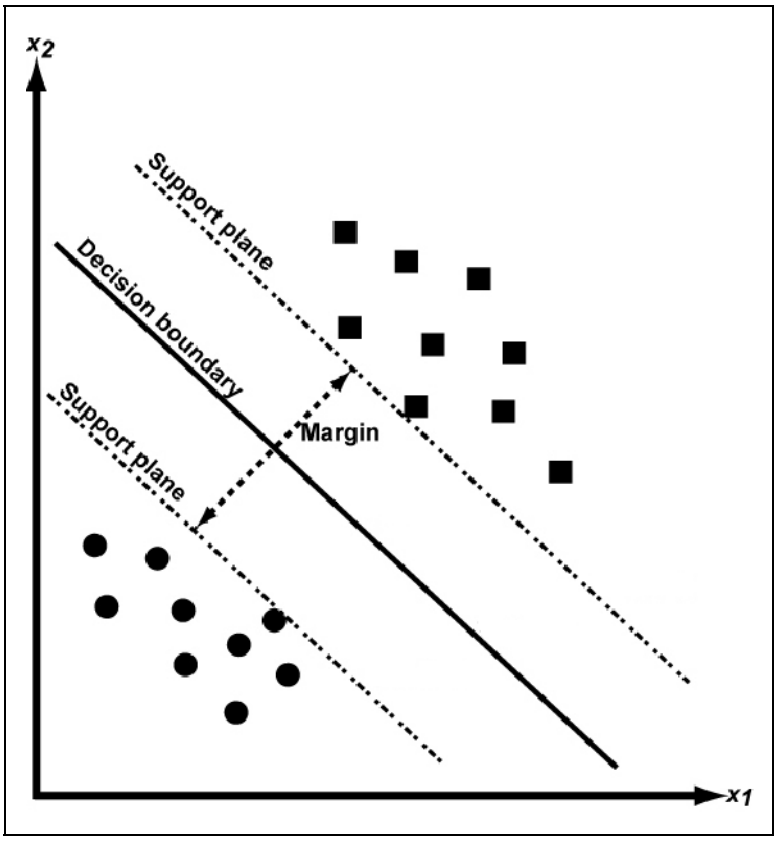

Figure 3. Support vector machine formulation for constructing a decision boundary. The decision boundary bisects support planes bounding the classes.

With all classification algorithms, a balance must be struck between obtaining good performance on the training data and generalizing to a test data set. An algorithm that classifies all training data correctly may

produce an overly complex decision boundary, which may not perform well on the test data. In the literature this is referred to as "bias-variance trade-off" and is addressed by constraining the complexity of the decision boundary (regularization). In cases such as linear discriminant analysis, the regularization is implicit in specifying the likelihood function. Alternatively, the complexity of the fit can be explicitly governed by regularization parameters (e.g., the width of kernels in a PNN or Lagrange multipliers in an SVM). These parameters are typically estimated from the training data using *cross-validation*, which sets aside a portion of the training data to assess classifier performance for a given regularization.

2.3. Examples of the dipole modeling approach

The polarization tensor formulation was used extensively within this project, for the following purposes:

1. To fit high-quality Geonics EM-61, Geonics EM-63, and Geophex GEM-3 data collected over a number of UXO and calibration items at the USACE ERDC test stand in Vicksburg, MS (see Report 3);
2. To fit magnetic, TEM, and frequency-domain electromagnetic (FEM) data collected over the Sky Research test plot in Ashland, OR (see Report 4).
3. To determine the improvement in performance of discrimination and cued-interrogation platforms developed under this project (see Report 5);
4. For the discrimination mode data collected at the Marine Corps Base Camp Lejeune, NC (see Report 8);
5. For the discrimination and cued-interrogation data collected at the Rocket Range and 20-millimeter (mm) Range Fan sites at the Former Lowry Bombing and Gunnery Range (FLBGR), CO (see Report 9);

Statistical classification methods were used to rank EM-61 and EM-63 data collected at Camp Lejeune and FLBGR.

3 Dipole-Based Fingerprinting Algorithm

As part of this project, a library- (or fingerprinting-) based technique was developed for the identification of UXO from time domain electromagnetic data. The high fidelity data acquired over a number of different ordnance items at the USACE ERDC test stand (see Report 3) were inverted for polarization tensors. The polarization tensors are functions of the target only and are used to characterize each member of the library. For each polarization tensor within the library, a template is generated. A template is defined as the data predicted by the polarization tensor that best fits the observed data. Generating this template requires solving a non-linear inverse problem for the orientation and location of a target. Each of the data templates is then compared to the observed data. To determine if the anomaly is likely generated by one of the targets, users can either find the template with the minimum error (for example, least squares) or the maximum correlation to the observed data. By not inverting for model parameters directly, tradeoffs between polarization tensor values and orientation and position can be avoided. This method is not meant to replace parametric inversion, but rather provides an additional analysis tool when working with data that do not support inverting for model parameters directly.

The objective of the template-matching analysis is to determine, from a list of M targets, the target that is most likely to have generated the observed data $\mathbf{d}^{obs}$. Each target in the list is characterized by model parameters, represented by the vector $\mathbf{p}^{t}_{i}$. Both dipole polarization parameters and SEA reduced source sets (RSS) are used for the vector of model parameters (see the next section for a discussion on SEA). For each $\mathbf{p}^{t}_{i}$ in the library, determine the location $\mathbf{r}_i$, orientation, represented by angles φ_i and θ_i and background characteristics $\mathbf{p}^{bg}$, which best fits the observed data $\mathbf{d}^{obs}$. The solution is determined by obtaining the maximum likelihood solution. The data predicted by this recovered model, $\mathbf{d}_i^{pred} = F[\mathbf{r}_i, \varphi_i, \theta_i, \mathbf{p}^{t}_{i}, \mathbf{p}^{bg}_{i}] = F[\mathbf{m}_i]$, are referred to as the template for target i. The target template $\mathbf{d}_i^{pred}$ that is most similar to the observed data $\mathbf{d}^{obs}$ is selected as the most likely target. A number of measures compare the target templates with the observed data, including measures of maximum correlation or minimum error. There are also several ways with which to define the minimum error. Riggs et al. (2001) outline the derivation of the minimum least squares

from a generalized likelihood ratio test (GLRT) with Gaussian data statistics. The likelihood ratio test for two targets is

$$\frac{p\left(\mathbf{d}^{\text{obs}} \mid \mathbf{p}_1\right)}{p\left(\mathbf{d}^{\text{obs}} \mid \mathbf{p}_2\right)} \underset{\text{target2}}{\overset{\text{target1}}{\lessgtr}} \frac{p(\mathbf{p}_2)(C_{01} - C_{11})}{p(\mathbf{p}_1)(C_{12} - C_{22})} \equiv \eta \tag{11}$$

where C_{ij} is the cost of classifying the target as p_i when the target is p_j , and $p(\mathbf{p}_i)$ is the prior probability for the i^{th} class. If the < condition applies, then target 1 is selected, otherwise target 2 is selected. The GLRT is obtained by substituting the maximum likelihood estimate into Equation 11. Considering two targets with equal prior probability of producing the anomaly, and assuming that an incorrect classification produces the same cost, $\eta = 1$. By taking the logarithm of the resulting expression, the decision criterion is to simply select the target that has the smallest least squares error:

$$\left\| V_d^{-1/2}\left(\mathbf{d}^{\text{obs}} - F(\mathbf{r}_1, \theta, \varphi, \mathbf{p}_1^t, \mathbf{p}_1^{bg})\right)\right\|^2 \underset{\text{target2}}{\overset{\text{target1}}{\lessgtr}} \left\| V_d^{-1/2}\left(\mathbf{d}^{\text{obs}} - F(\mathbf{r}_2, \theta, \varphi, \mathbf{p}_2^t, \mathbf{p}_2^{bg})\right)\right\|^2 \tag{12}$$

where $\mathbf{r}_i$ is the position, and θ_i and φ_i are the orientation angles that produce the best fits of the observed data for the model $\mathbf{p}^t_i$. For multiple candidate targets, simply choose the target with the smallest least squares misfit.

A blind test of the prototype library/template matching code was performed using data collected over 10 items in the Sky Research test site (see Report 4). Data were collected in both dynamic and cued-interrogation modes (Figure 4). Dynamic data were collected using a push-cart along transects separated by 0.5 meter (m). Cued-interrogation data were collected by placing a Geonics EM-63 sensor without wheels on a portable test stand positioned over the target. When performing the template-matching algorithm on the dynamically collected data, 8 of 10 items were correctly identified (Table 1). When processing the statically collected data, 9 of 10 items were correctly identified.

a. Dynamic data collection

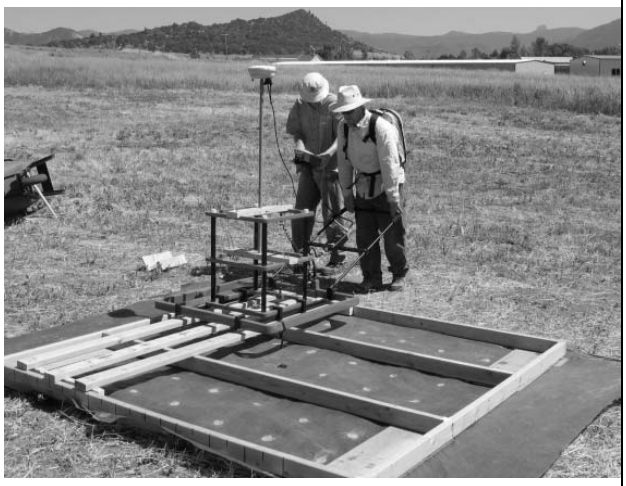

b. Cued (Static) Data collection

Figure 4. Two EM-63 data collection modes.

Table 1. Results when applying the Fingerprinting/Template matching algorithm to dynamic and cued-interrogation style data.

Cell Label	Target Description	Predicted Target	
		Dynamic Data	Cued-interrogation
56d	40-mm M385	✓ 40-mm M385	✓ 40-mm M385
57b	BDU-28 submunition	✓ BDU-28 submunition	✓ BDU-28 submunition
60	81-mm M374 mortar	✓ 81-mm M374 mortar	✓ 81-mm M374 mortar
64c	M42 submunition	✓ M42 submunition	✓ M42 submunition
65a	MK 118 Rockeye	✓ MK 118 Rockeye	× 40-mm M385
67	2.75-in. rocket	✓ 2.75-in. rocket	✓ 2.75-in. rocket
68	2.75-in. rocket	✓ 2.75-in. rocket	✓ 2.75-in. rocket
71	M456 Heat Rd	× MN 76 mm	✓ M456 Heat Rd
72b	BLU-26 submunition	× M42 submunition	✓ BLU-26 submunition
73b	60-mm M493A	✓ 60-mm M493A	✓ 60-mm M493A

Observed and predicted data when applying the library method to dynamically collected data measured over a 76-mm projectile are compared in Figure 5. The data predicted using the 76-mm projectile polarization parameters from the library produce the smallest misfit.

When processing the cued-interrogation data, the background response needs to be taken into account due to the close proximity of the transmitter coil to the ground. Since the data were collected over a 1.8-m^2 area, a high pass filter could not be used to remove the background response. Therefore when solving for the least squares misfit of each library target, a background soil model was included. Figure 6 shows the misfit for data collected over an MK118 Rockeye. The MK118 Rockeye was the only UXO incorrectly identified by the template-matching algorithm when applied to cued-interrogation data. The incorrect identification may be related to a trade-off between the parameter modeling the relatively large background soil signal in the data (approximately 20 mV in the first time channel) and the polarization tensor. In addition, the anomaly was only partially sampled due to the test stand not being centered on the target; therefore fewer data were available to constrain the result.

Full details of the method are presented in Pasion et al. (2007).

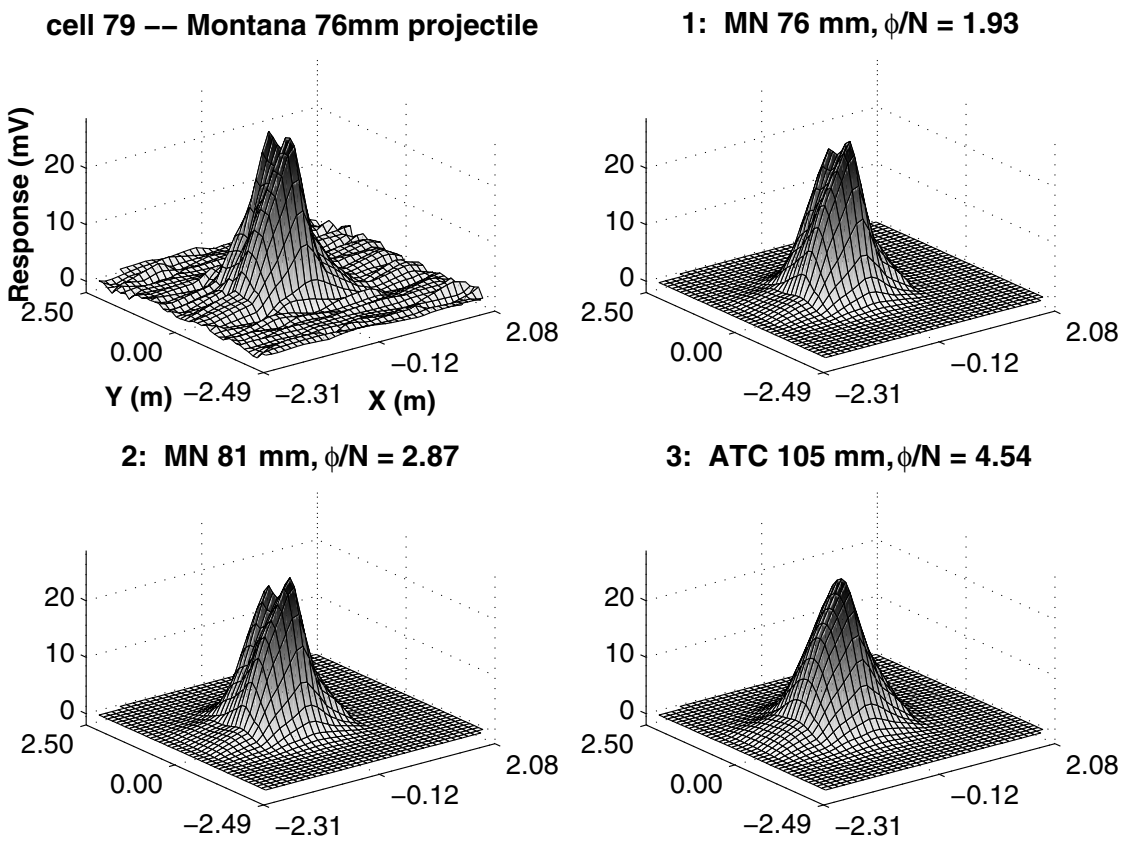

a. The upper left panel contains the fifteenth time channel of observed data. The remaining panels represent the three most likely targets, ranked according to the normalized misfit φ/*N*.

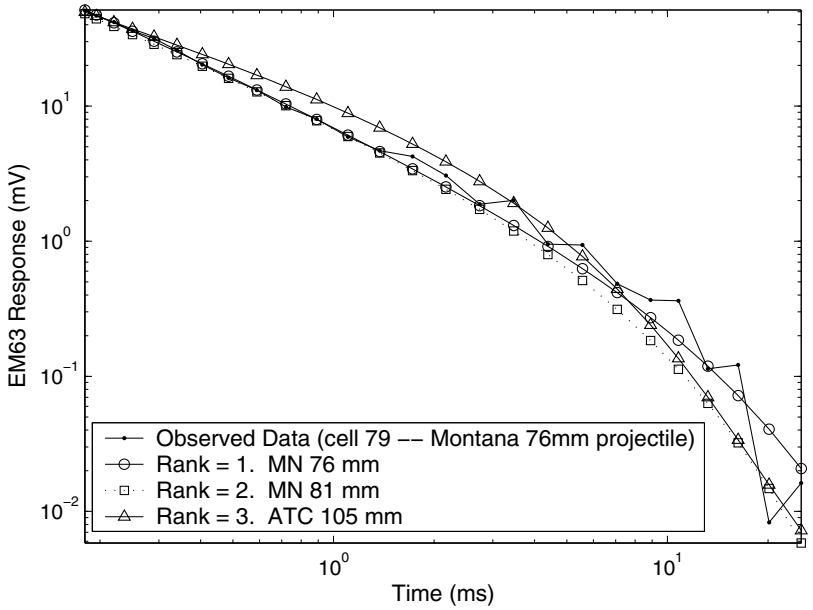

b. The best fit soundings observed at a point directly over the rocket.

Figure 5. Application of the library method to dynamically collected data measured over a 76-mm mortar. The objective is to determine which target in the library most likely fits the data.

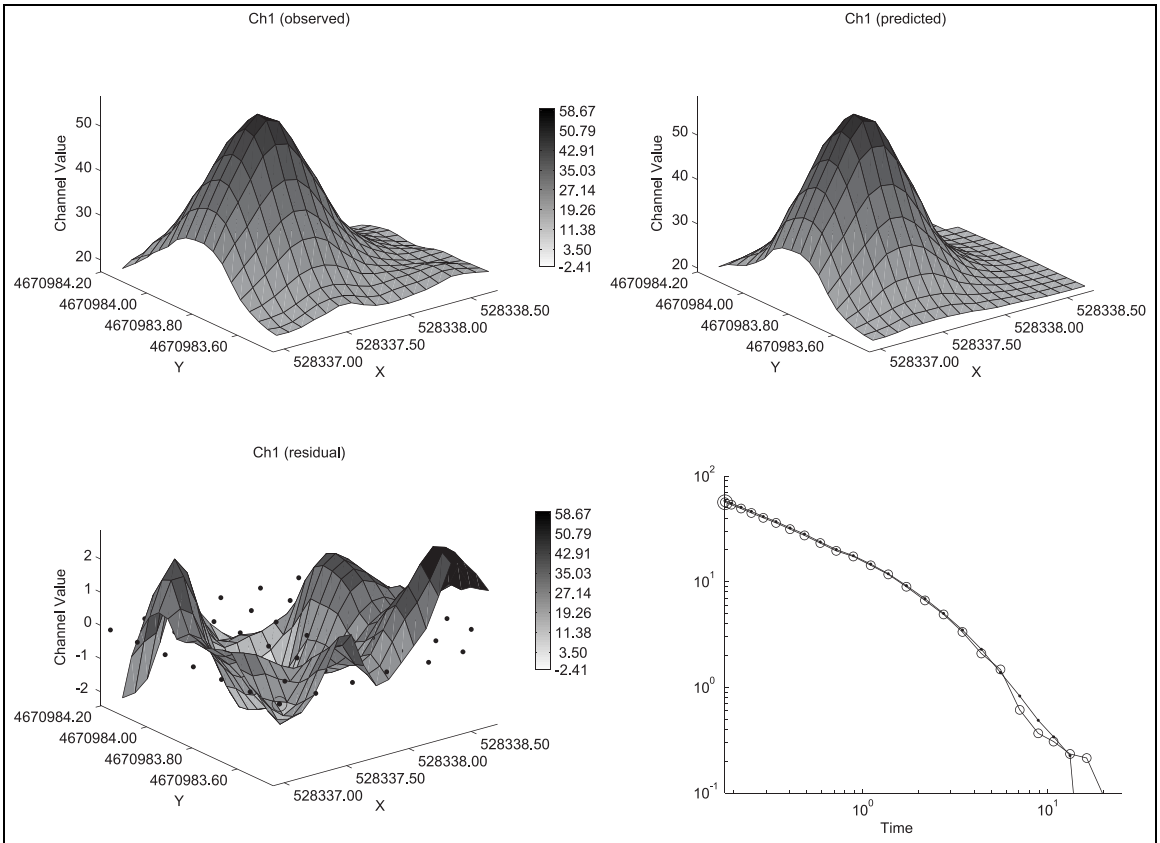

a. UXO Lab output of data fit for the first time channel. Note that at the edges of the data there is approximately a 20-mV response due to the soil.

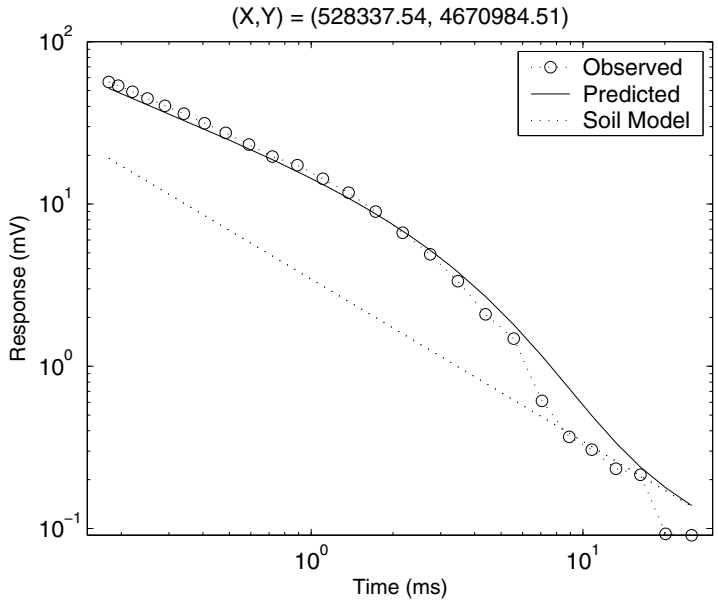

b. Data misfit for a sounding taken directly over an MK118 Rockeye. The estimated soil noise is of approximately the same order as the data, causing difficulty in correctly identifying the target.

Figure 6. Application of the library method to data collected in a cued-interrogation mode over an ATC MK118. The close proximity of the transmitter coil to the ground introduces a significant soil response.

4 Standardized Excitation Approach

The Standardized Excitation Approach (SEA) is a numerical technique for computing the EMI response from a three-dimensional, electromagnetically heterogeneous object in both near and far fields. The objective of the SEA is to determine a set of characteristic sources, called the Reduced Set of Sources (RSS), associated to each UXO. These sources can then be used for fast modeling of the EMI response. The full EMI solution is obtained by the superposition of responses to the spheroidal excitation modes. A potential advantage of the SEA approach over that of the dipole model, is that it is able to reproduce the signal from an arbitrary body at an arbitrary orientation and distance (both near- and far-field).

Under the quasi-magnetostatic approximation, the magnetic field outside of an object is irrotational. For a primary field, the related primary potential ψ^{pr} on a fictitious spheroid $\xi = \xi_0$ surrounding the object can be expressed as:

$$\psi^{pr}(\eta,\xi,\varphi) = \frac{H_0 d}{2} \sum_{m=0}^{\infty} \sum_{n=m}^{\infty} \sum_{p=0}^{1} b_{pmn} P_n^m(\eta) P_n^m(\xi) T_{pm}(\varphi) \qquad (13)$$

where (η,ξ,φ) are the standard prolate spheroidal coordinates, d is the inter-focal distance, P_n^m are associated Legendre functions of the first kind (Shubitidze et al. 2005b), and $T_{pm}(\varphi)$ is $\cos(m\varphi)$ for $p = 0$ and is $\sin(m\varphi)$ for $p = 1$. The coefficients b_{pmn} can be determined from the known primary field or potential. Note that a spheroid is chosen because it can assume the general shape of an elongated object of interest, typically BOR. Equation 13 is a decomposition of a primary magnetic field $(-\Delta\psi^{pr})$ into spheroidal modes. Note that the lower primary field modes $(p, m, n) = (0, 0, 1), (0, 1, 1), (1, 1, 1)$ correspond to uniform excitation in the z, x, and y directions, respectively.

After the primary magnetic field is decomposed into fundamental spheroidal modes, the secondary field due to an object can be written as a linear superposition of an object's response for each pmn excitation mode, i.e.,

$$\mathbf{H}_{sc}(\mathbf{r}) = \sum_{m=0}^{\infty}\sum_{n=m}^{\infty}\sum_{p=0}^{1} b_{pmn}\sum_{i=1}^{N_{red}} q_i^{pmn}\mathbf{G}(\mathbf{r},\mathbf{r}_i') \tag{14}$$

where $\mathbf{r}$ is the position vector of an observation point outside of the object and q_i^{pmn} is the strength in the secondary field for the pmn mode at the i^{th} point $\mathbf{r}_i'$ distributed on a spheroidal surface and called the reduced set of source (RSS, Shubitidze et al. 2005b), and $\mathbf{G}(\mathbf{r},\mathbf{r}_i')$ is the Green's function for the magnetic field given by

$$\mathbf{G}(\mathbf{r},\mathbf{r}_i') = \frac{1}{4\pi\mu_0}\frac{\mathbf{r}-\mathbf{r}_i'}{\left|\mathbf{r}-\mathbf{r}_i'\right|^3}. \tag{15}$$

It is observed from Equation 14 that the extrinsic characteristics in the secondary field are contained in the spheroidal modal expansion coefficients b_{pmn} determined by an excitation type, the location and orientation of the target, while the intrinsic characteristics of field response are separated in the RSS determined by the target's geometry and physics. This property of the RSS can make the SEA appealing to build libraries for the purpose of discrimination and classification regardless of what excitation is used.

There are two ways of determining q_i^{pmn}. One is to formulate the problem as an inverse problem and determine q_i^{pmn} for each mode, given the measured data. Obviously this process requires very detailed, low-noise measurements, as well as techniques to reduce the problem of ill conditioning.

Another method of determining q_i^{pmn} is a forward process that determines the amplitude q_i^{pmn} assuming that the geometry of an object and its physical properties are known. In this procedure (Shubitidze et al. 2005b), q_i^{pmn} can be determined by solving the following linear equation:

$$[g]\left[q^{pmn}\right] = \left[\Psi_{pmn}^{sc}(\mathbf{r}_j)\right] \tag{16}$$

where:

$$g(\mathbf{r}_j, \mathbf{r}_i') = \frac{1}{4\pi\mu_0} \frac{\mathbf{1}}{\left|\mathbf{r}_j - \mathbf{r}_i'\right|} \tag{17}$$

is the potential at the $\mathbf{r}_j$ observation point produced by the i^{th} point magnetic charges at $\mathbf{r}_i'$ on the auxiliary surface where the q_i^{pmn} are located. $\psi_{pmn}^{sc}\left(\mathbf{r}_j\right)$ is the scalar potential at $\mathbf{r}_j$ for the pmn mode with $b_{pmn} = 1$ and is given by

$$\left[\psi_{pmn}^{sc}\left(\mathbf{r}_j\right)\right] = \sum_{k=1}^{N} Q_k^{pmn} \frac{1}{4\pi\mu_0} \frac{\mathbf{1}}{\left|\mathbf{r}_j - \mathbf{r}_k'\right|} \tag{18}$$

In Equation 18, Q_k^{pmn} is the strength of the k^{th} auxiliary magnetic charge, located at $\mathbf{r}_k'$ inside the object. The quantity can be determined by the method of auxiliary sources (MAS, Shubitidze et al. 2003). Therefore, the SEA adopted here for establishing these libraries needs to deal with the geometry of an object and estimate its conductivity and permeability.

4.1. Template matching using GEM-3 data

Full implementation of the SEA fingerprinting method would involve solving for the position and orientation that minimized the least-squares difference between the observed data and that predicted from each item in the library. The code for inverting for location and orientation is being developed and is not mature enough to implement the nonlinear inversion approach. Therefore, a template-matching technique was developed to determine depth and orientation by searching a library of data pre-modeled at several depths and dip angles. Image registration was used to find the location and azimuth angle of the target. The main objective of implementing this style of template matching is to determine if it is possible to identify targets using an RSS library without a priori information.

The first step of the algorithm is to generate a library of UXO responses. Generating a library of UXO responses meant that all forward modeling using the RSS only needed to be performed once, thereby increasing the speed of the analysis. Target responses for nine ordnance items were calculated for target distances from the GEM-3 sensor head varying, at

10-centimeter (cm) intervals, from 20 cm to 80 cm. At each depth the target was measured at dip angles from 0 degrees (horizontal) to 90 degrees (vertical), at 15-degree intervals. Data were modeled on a 1-m² area and on a uniform grid with 10-cm spacing. UXO identification is achieved by determining the data template from the library that best matches the sensor data, by cycling through each of the data templates. However, the target location and azimuthal orientation are unknown. Determining the target location and azimuthal orientation is equivalent to determining the translation and rotation of the data templates. This operation represents a simple problem in image registration, since there is no need to consider scaling the template.

The above procedure was demonstrated with GEM-3 data collected on the USACE ERDC Test Stand (see Report 3). A first example compares data from a horizontal 40-mm projectile located 30 cm from the GEM-3 sensor head. Figure 7a compares the sounding directly over the center of the target. Figure 7b compares the misfit values for the various items in the RSS library. It is clear that C3 is the most likely target. The ease with which the algorithm picked C3 is, in part, due to C3 being the only non-ferrous (aluminum) item in the library.

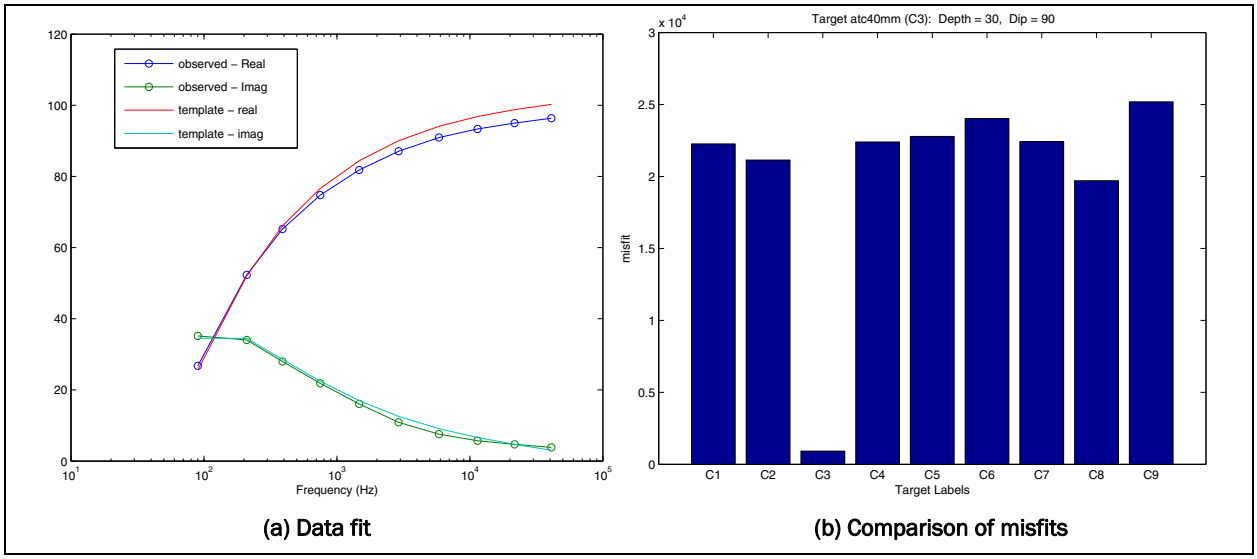

Figure 7. 40-mm projectile example.

Figure 8 plots the results when the data from an 81-mm mortar (M374) are fit. Although the correct target (C8) has the minimum misfit, several other targets have relatively similar misfit values, indicating that several targets appear quite similar when viewed by a GEM-3 sensor 50 cm from the target.

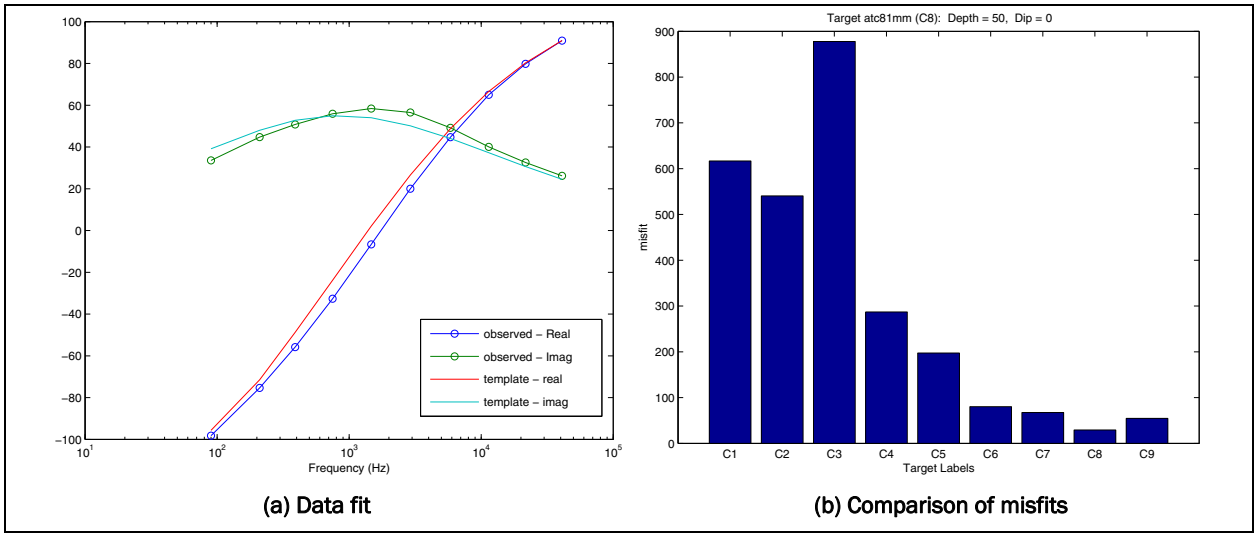

(a) Data fit (b) Comparison of misfits

Figure 8. 81mm mortar example.

4.2. Preliminary results using Geonics EM-63 data

The SEA methods were extended to time domain measurements and preliminary results obtained from EM-63 test stand data are presented here. The first example considered a solid steel cylinder with a length L of 30.48 cm and a diameter d of 7.5 cm. The cylinder was oriented at three polar angles of $\theta = 0°, 5°, 90°$. For each of the three excitations, the vertical distance between the sensor and the center of the cylinder h was 60 cm. Applying the SEA procedure produced the associated transient responses. The comparisons in Figures 9a–9c show that the measured and modeled TEM decay curves agree well. Good agreement is also observed in the two-dimensional (2D) response image of Figure 10 at times t_1 = 0.18 microseconds (ms) and t_7 = 0.41 ms.

In the second example, an ATC 40-mm projectile (aluminum) with length of L = 75 mm was used. The sensor and object configurations are the same as that of the cylinder case. Figures 11 and 12 show the measured and modeled TEM decay curves and the 2D response image at two instances in time. The SEA again produced the TEM response very well except for a small anomaly in the axial response, which was determined to be related to an instrument artifact within the EM-63 sensor.

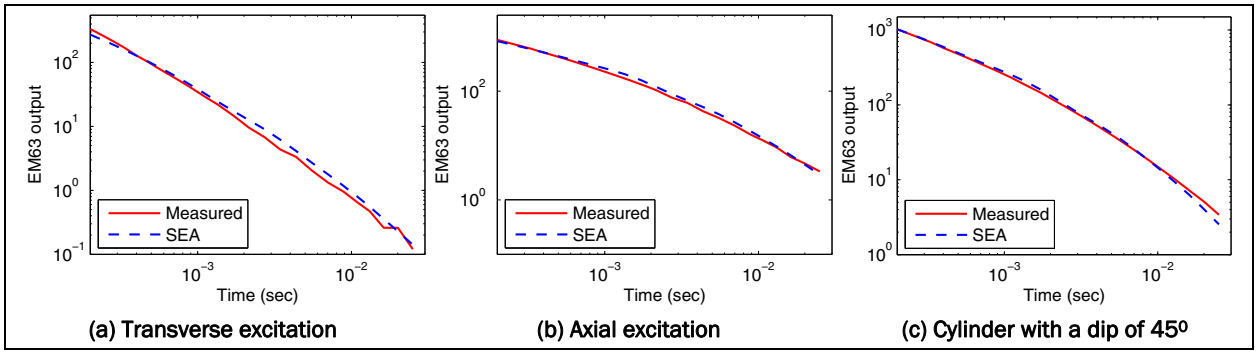

Figure 9. TEM response from a solid steel cylinder: L = 30.48 cm, d = 7.5 cm.

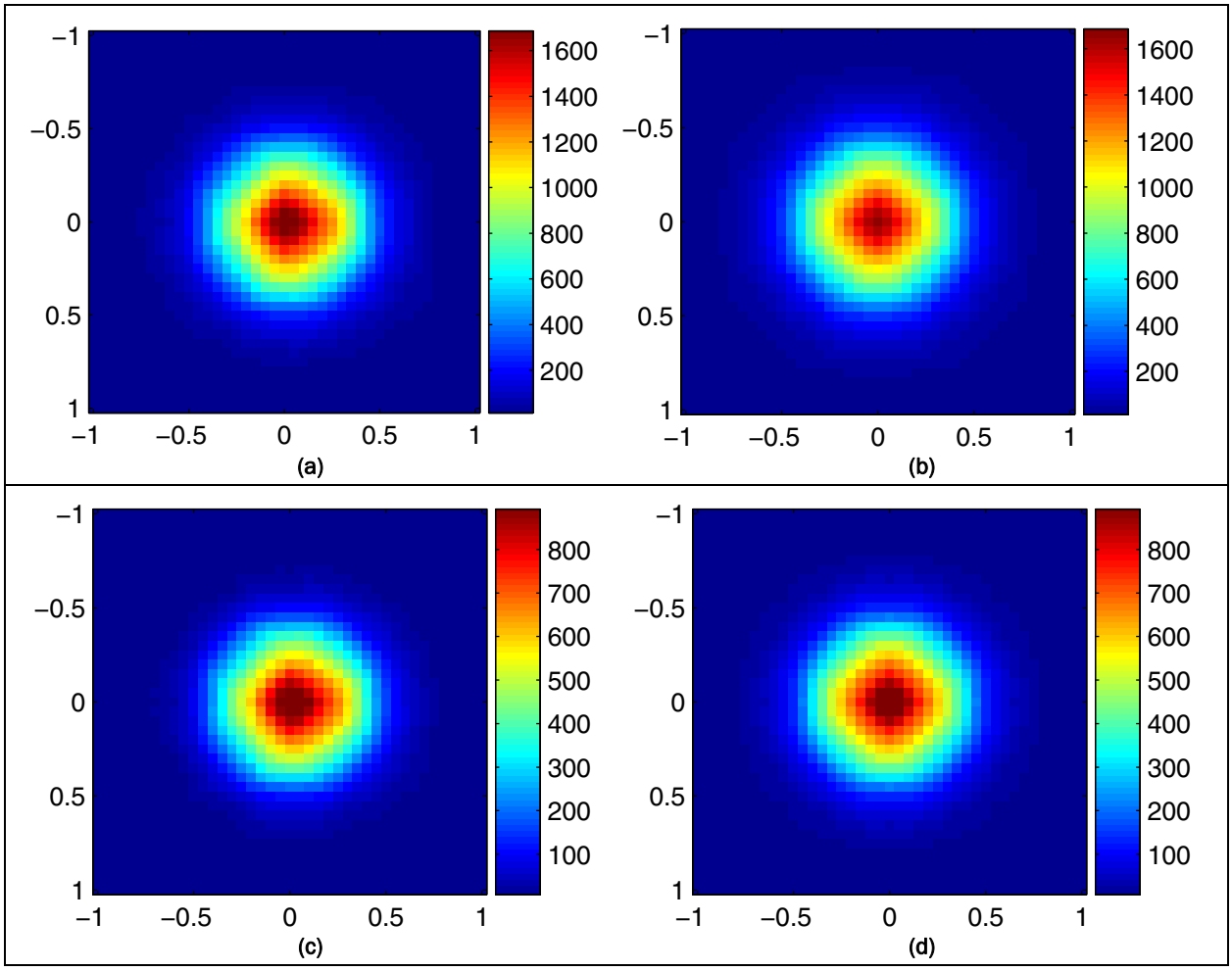

Figure 10. 2D TEM response at instant time from the solid steel cylinder: Axial excitation. t_1 = 0.18 ms: Measured (a) and the SEA (b). t_7 = 0.41 ms: Measured (c) and the SEA (d).

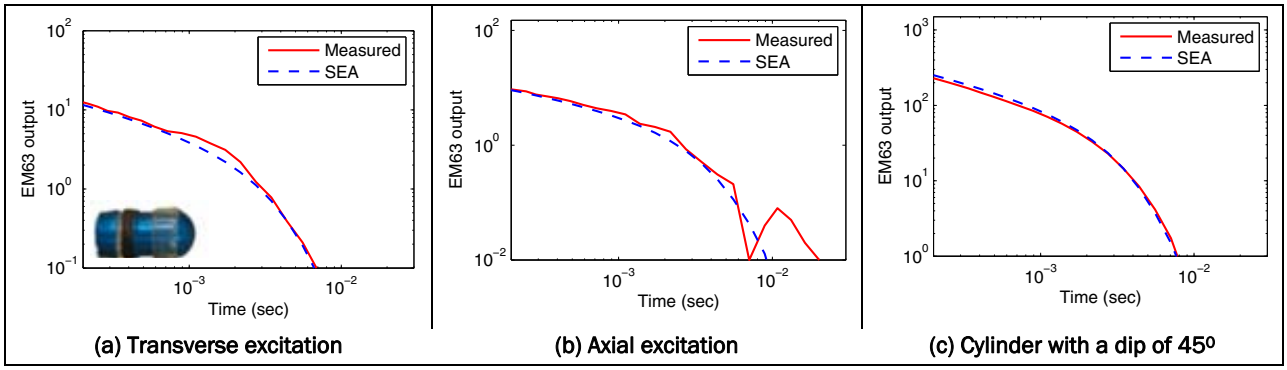

Figure 11. TEM response from ATC 40-mm aluminum: *L* = 75 mm.

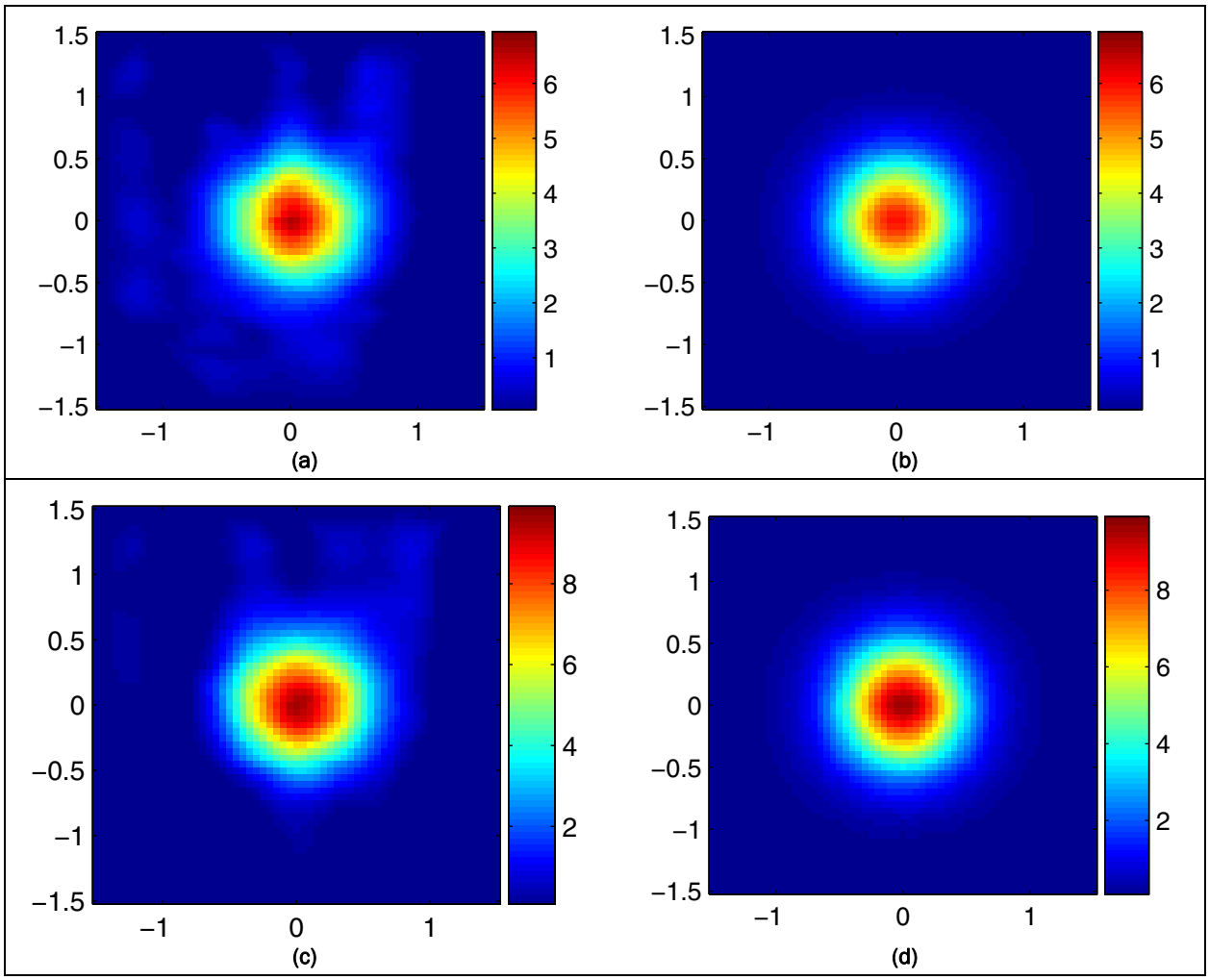

Figure 12. 2D TEM response at instant time from ATC 40 mm: Axial excitation. t_1 = 0.18 ms: Measured (a) and the SEA (b). t_7 = 0.41 ms: Measured (c) and the SEA (d).

The test stand data illustrate that the formulated SEA procedure can be used to accurately simulate various scenario measurements of transient field or voltage due to a metallic object at either on-time or off-time for an arbitrary transmitter waveform. The results presented using the test stand EM-63 data illustrated the effectiveness of the approach. As the procedure is able to produce full three-dimensional (3D) TEM responses of an object for a given TEM system, it is desirable to build up a responding source library in time-domain for the purpose of UXO discrimination. With such a pre-calculated time-domain library, one can rapidly conduct a finger-printing test of TEM data for known candidates using the SEA without the need for additional transformations.

More details on the theoretical development of the SEA method can be found in Pasion et al. (2006) and Song et al. (2008).

5 Surface Magnetic Charge

The Surface Magnetic Charge (SMC) model (Shubitidze et al. 2005a) proposes a simple physical framework for describing the response of a metallic object to an inducing electromagnetic field. Like the SEA approach, it is applicable in both the near and far fields. However, in contrast to the SEA, the SMC is a parameter estimation technique and not a fingerprinting method. Thus, statistical or rule-based classification would need to be applied to the estimated parameters in order to determine the UXO likelihood of an unknown, buried object.

The SMC model assumes a highly conducting, permeable, arbitrarily shaped, heterogeneous metallic target embedded in a soil with low conductivity (< 1 S/m). In a quasi-magneto static regime, displacement currents are negligible, conduction currents are weak outside the target, and the magnetic field is irrotational and can be written as the gradient of a scalar potential ψ:

$$\mathbf{H}^{\mathbf{sc}}(\mathbf{r},\xi) = -\nabla\psi^{sc}(\mathbf{r},\xi) \tag{19}$$

where the variable ξ can represent either time t or frequency ω. If Gauss' Law is assumed for the magnetic field and if it is assumed that the field is generated by surface charges σ_m only, the magnetic field is given by:

$$\mathbf{H}^{\mathbf{sc}}(\mathbf{r},\xi) = \frac{1}{4\pi\mu_o}\int_S \sigma_m(\mathbf{r}',\xi)\frac{(\mathbf{r}-\mathbf{r}')}{|\mathbf{r}-\mathbf{r}'|^3}dS' \tag{20}$$

where $\mathbf{r}$ is the observation point, $\mathbf{r}'$ the source point, S is a closed surface surrounding the scatterer, and μ_0 is the magnetic permeability of free space.

To numerically solve the SMC integral and define a charge distribution that characterizes a given type of ordnance, the surface S is split in subsurfaces Δs_i assuming that the amplitude of σ_i, the surface magnetic charge at the center of Δs_i, is proportional to the normal component of the incident primary magnetic field at that point:

$$\sigma_i(\mathbf{r}',t) = q_i(\mathbf{r}',t)\left[\mathbf{H}^{\mathbf{pr}}(\mathbf{r}')\cdot\hat{\mathbf{n}}(\mathbf{r}')\right] = q_i(\mathbf{r}',t)\,H_n^{pr}(\mathbf{r}') \tag{21}$$

where q_i is the normalized magnetic charge surface density, assumed to be independent of the relative position of the sensor and target (Equation 12). Integration over the surface S defines the total normalized surface magnetic charge (NSMC) of an object at a given time channel (or frequency) as:

$$Q(t) = \sum_{i=1}^{N} q_i(\mathbf{r}', t)\Delta S_i \tag{22}$$

5.1. Preliminary results using Geonics EM-63 data

In Pasion et al. (2006) the SMC model was applied to the UXO problem, with the result that the SMC provided accurate data prediction and demonstrated potential for discrimination of a large collection of standard UXO. As an example, regularized inversion and detailed analysis are applied to data for 40-mm, 60-mm, 90-mm, and M42 standard ordnance at multiple depths and orientations. The Geonics EM-63 sensor acquired data on the USACE ERDC Vicksburg test stand at 26 time channels (0.18 ms to 25.14 ms), two depths (one shallow, one deep) and three inclinations (0, 45, 90 degrees). Figure 13 shows the total magnetic charge as a function of time for all measured configurations obtained with the proposed regularized inversion algorithm for NSMC. Several conclusions can be drawn:

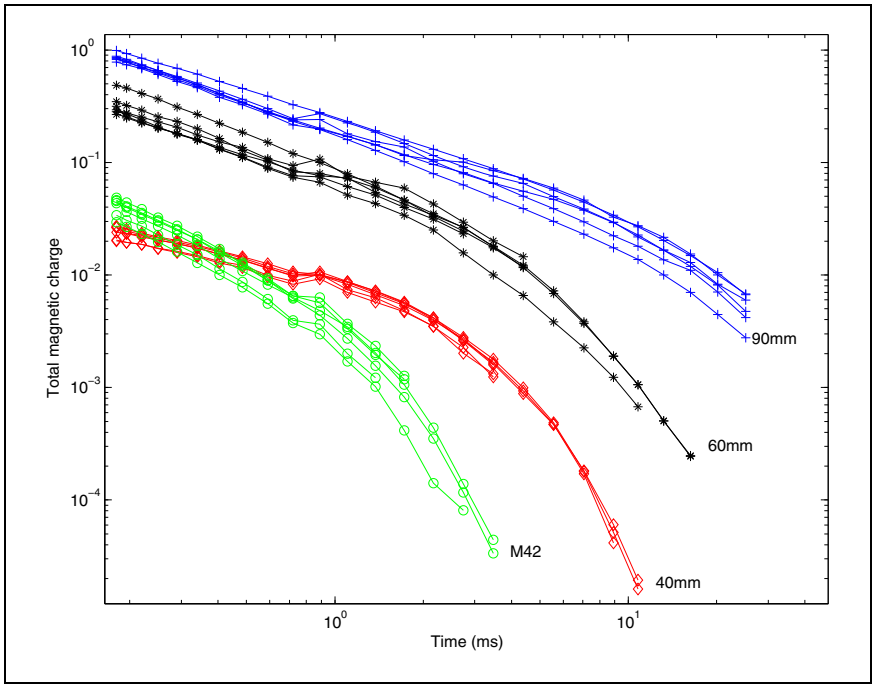

Figure 13. The total normalized magnetic charge for 40-mm, 60-mm, 90-mm, and M42 standard ordnance at multiple depths and orientations.

- All lines cluster for each object; the recovered total magnetic charge is therefore a stable feature and the inversion is robust.
- Each object has a distinct time-evolving total magnetic charge.
- The magnitude of the total magnetic charge scales with the volume of the object.
- Objects with different physical properties have different time decays for the total magnetic charge, as illustrated by the M42 and 40-mm items that have similar size but different material.

These results suggest clear and stable separation with NSMC and the total magnetic charge for these four types of ordnance, thus opening the possibility of applying automated discrimination procedures. As a side note, there is a slight increase of the total magnetic charge for the 10th and 11th time channels. This effect is only due to a pervasive instrument bias, not to any physical property or modeling issue, and would not appear should the sensor be perfectly calibrated.

Figure 14 extends the picture further, showing results for a wider range of targets, including pieces of scrap as well as a variety of cylindrical calibration objects. Even with the expanded set of targets, the total magnetic charge (TMC) for each item is unique enough to make discrimination between object types feasible (at least on data with dense coverage, high signal-to-noise ratio (SNR), and accurate positioning).

5.2. Preliminary results using Geophex GEM-3 data

The SMC method was also tested on the GEM-3 data collected at the ERDC test stand (see Report 3). Data were processed and inverted by taking the modulus of data for every time channel so that amplitude reached a maximum value directly above target. TMC is computed for each item at each frequency. Figure 15 shows that each type of ordnance has a distinct distribution of TMC over the measured range of frequencies, independent of its relative position with the sensor. This indicates the potential for discrimination of ordnance by TMC.

More details on the theoretical development of the SMC method can be found in Pasion et al. (2006) and Lhomme et al. (2007).

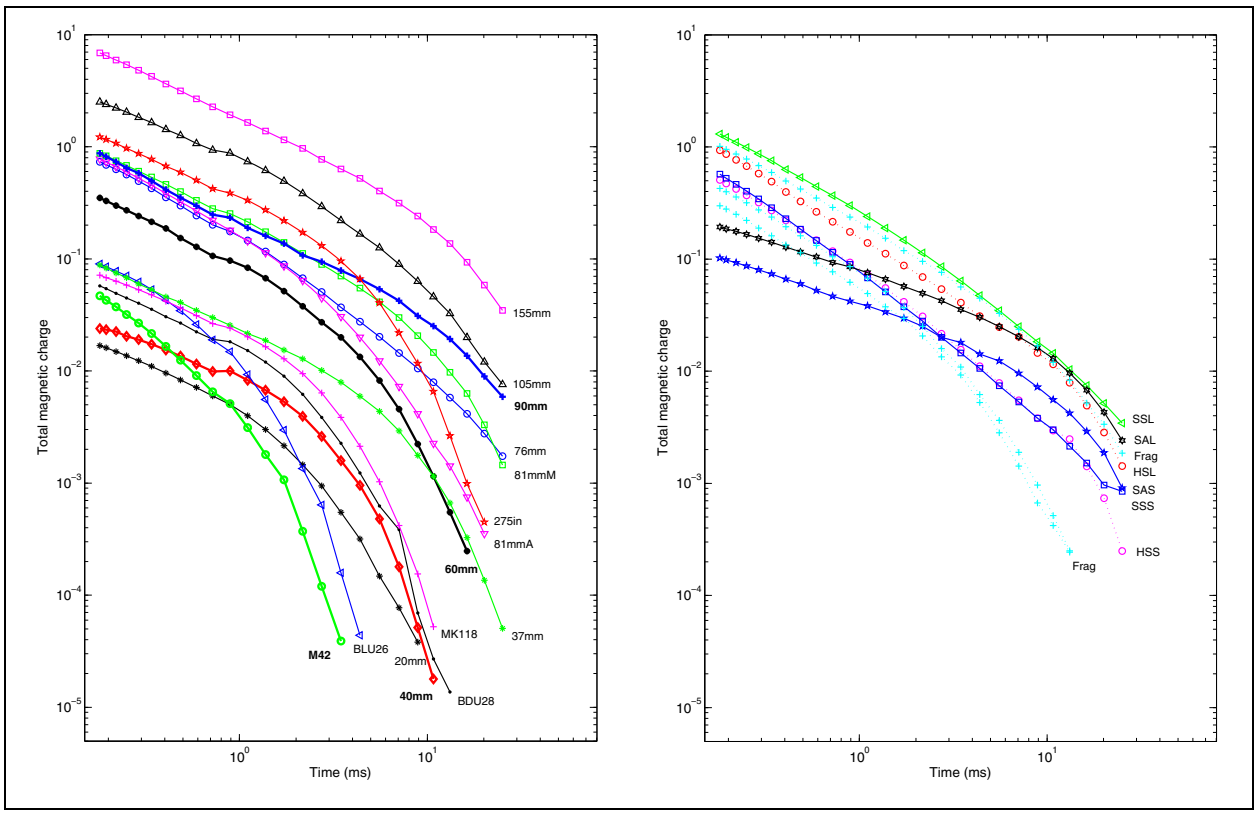

Figure 14. Total magnetic charge recovered from EM-63 data collected over a range of different ordnance (left) and cylinders (right).

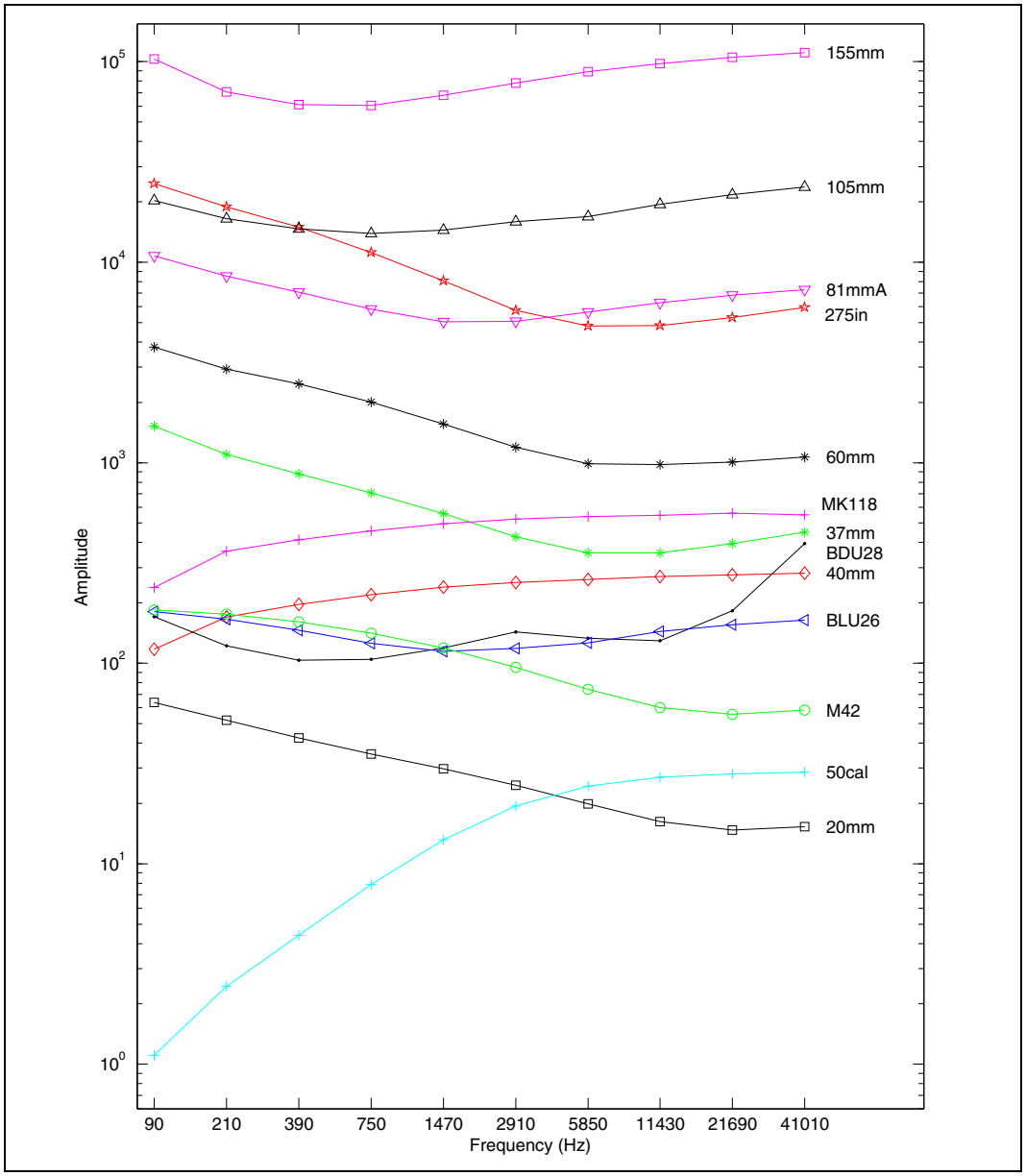

Figure 15. Total magnetic charge of 13 standard UXO items as a function of frequency, for data acquired with a GEM-3 sensor over Vicksburg test stand. Only median is shown for clarity.

6 Conclusions

This report describes the various forward models and inversion procedures that are used to aid UXO discrimination from magnetic and time- and frequency-domain electromagnetic data. The simplest and most widely used magnetic and EMI models are based on dipoles: a static dipole in the magnetic case, and a polarization tensor formulation for EMI. The dipole model parameters can act as feature-vector inputs to a statistical or rule-based classification scheme to determine their UXO likelihood. Alternatively, high-quality test-stand data can be used to create a library of polarization tensor models and implement a template or fingerprint-matching scheme to determine the identity of each buried object. Both of these dipole-based methods are well developed and were used extensively in this project. In addition, the methods are undergoing test and evaluation at a number of live sites through the ESTCP program.

The advantage of the SEA and SMC methods is that, unlike the dipole model, they are able to reproduce the response of an object in both the near and far fields. However, the methods are not yet as mature as the dipole model, and the work described herein must be considered preliminary. Neither method can currently be used for discrimination of live-site data. In addition, neither method has demonstrated a clear, practical advantage over the dipole-based methods at this time.

References

Bell, T. H., B. J. Barrow, and J. T. Miller. 2001. Subsurface discrimination using electromagnetic induction sensors. In *IEEE Transactions on Geoscience and Remote Sensing* 39:1286–1293.

Beran, L., S. D. Billings, and D. W. Oldenburg. 2004. A comparison of classification algorithms for UXO discrimination. In *Proceedings of the 2004 UXO Forum*, St. Louis, March 9–12, 2004.

Billings, S. D. 2004. Discrimination and classification of buried unexploded ordnance using magnetometry. In *IEEE Transactions of Geoscience and Remote Sensing* 42:1241–1251.

Billings, S. D., L. R. Pasion, and D. W. Oldenburg. 2002a. Inversion of magnetics for UXO discrimination and identification. In *Proceedings of the 2002 UXO Forum*, Orlando, September 2002.

Billings, S. D., L. R. Pasion, and D. W. Oldenburg. 2002b. *Discrimination and identification of UXO by geophysical inversion of total-field magnetic data*. ERDC/GSL TR-02-16. Vicksburg, MS: U.S. Army Engineer Research and Development Center.

Collins, L., Y. Zhang, J. Li, H. Wang, L. Carin, S. Hart, S. Rose-Phersson, H. Nelson, and J. R. McDonald. 2001. A comparison of the performance of statistical and fuzzy algorithms for unexploded ordnance detection. In *IEEE Transactions on Fuzzy Systems* 9:17–30.

Gasperikova, E., J. T. Smith, F. Morrison, and A. Becker. 2006. Berkeley UXO discriminator (BUD) for UXO detection and discrimination. In *Partners in Environmental Technology Technical Symposium and Workshop*, November 2006.

Hart, S. J., R. E. Shaffer, S. L. Rose-Pehrsson, and J. R. McDonald. 2001. Using physics-based modeler outputs to train probabilistic neural networks for unexploded ordnance (UXO) classification in magnetometry surveys. In *IEEE Trans. Geosci. Remote Sensing* 39(4):797–804.

Lhomme, N., L. P. Pasion, and D. W. Oldenburg. 2007. Identification of UXO with surface magnetic charges on a sphere. In *Symposium on the Application of Geophysics to Engineering and Environmental Problems*, Denver, CO, April 1–5.

Miller, J. T., T. H. Bell, J. Soukup, and D. Keiswetter. 2001. Simple phenomenological models for wide-band frequency domain electromagnetic induction. In *IEEE Transactions on Geoscience and Remote Sensing* 39:1294–1298.

Pasion, L. P., and D. Oldenburg. 2001a. A discrimination algorithm for UXO using time domain electromagnetics. *Journal of Engineering and Environmental Geophysics* 28:91–102.

Pasion, L. R., and Oldenburg, D. W. 2001b. Locating and characterizing unexploded ordnance using time domain electromagnetic induction. ERDC/GSL TR-01-10. Vicksburg, MS: U.S. Army Engineer Research and Development Center.

Pasion, L. R., S. D. Billings, and D. W. Oldenburg. *Guidelines on data quality requirements for advanced discrimination of UXO*. Technical Report (in preparation). Project Number DACA42-03-P-0238. Vicksburg, MS: U.S. Army Engineer Research and Development Center.

Pasion, L. P., S. D. Billings, D. W. Oldenburg, and S. E. Walker. 2007. Application of a library based method to time domain electromagnetic data for the identification of unexploded ordnance. *Journal of Applied Geophysics* 61(3-4):279–291.

Pasion, L. P., N. Lhomme, L. P. Song, F. Shubitidze, and D. W. Oldenburg. 2006. A unified approach to UXO discrimination using the Method of Auxiliary Sources. *SERDP-UX-1446 Final Report*.

Riggs, L., J. Mooney, and D. Lawrence. 2001. Identification of metallic mine-like objects using low frequency magnetic fields. In *IEEE Transactions on Geoscience and Remote Sensing* 39(1)56–66.

Shubitidze, F., K. O'Neill, I. Shamatava, K. Sun, and K. Paulsen. 2005a. A simple magnetic charge model for classification of multiple buried metallic objects in cases with overlapping signals. In *Proceedings from SAGEEP 05*.

Shubitidze, F., K. O'Neill, I. Shamatava, K. Sun, and K. D. Paulsen. 2005b. Fast and accurate calculation of physically complete EMI response by a heterogeneous metallic object. In *IEEE Transactions of Geoscience and Remote Sensing* 43:1736–1750.

Shubitidze, F., K. O'Neill, K. Sun, I. Shamatava, and K. D. Paulsen. 2003. A hybrid full MAS and combined MAS/TSA algorithm for electromagnetic induction sensing: *Applied Computational Electromagnetics Society Journal* 19:112–126.

Song, L, F. Shubitidze, L. R. Pasion, D. W. Oldenburg, and S. D. Billings. 2008. Computing transient electromagnetic response of a metallic object with a Spheroidal Excitation Approach. In *IEEE Transactions on Geoscience and Remote Sensing* 5(3):359–363.

Zhang, Y., L. M. Collins, and L. Carin. 2003a. Model-based statistical signal processing for UXO discrimination: Performance results from the JPG-V demonstration. In *Proceedings of SPIE* 5089:1116–1126.

Zhang, Y., L. Collins, H. Yu, C. E. Baum, and L. Carin. 2003b. Sensing of unexploded ordnance with magnetometer and induction data: Theory and signal processing. In *IEEE Trans. Geosci. Remote Sensing* 41:1005–1015.

Zhang, Z., X. Liao, and L. Carin. 2004. Detection of buried targets via active selection of labeled data: Application to sensing subsurface UXO. In *IEEE Transactions on Geoscience and Remote Sensing* 42:2535–2543.

Appendix A: Some Characteristics of the Dipole Model

A.1. The relationship between a horizontal loop Tx and the transverse and axial

The general approach to processing of EM data is to invert data for model parameters that are representative of the physical characteristics of the target. The ability to resolve the various polarization components is directly related to the ability of the transmitter loop to illuminate both polarizations. The optimal sensor for this purpose would generate a primary field that illuminates the target at a number of angles. This can be accomplished through multiple transmitter loops. Although such instrumentation is under development (for example Gasperikova et al. 2006), most sensors use a horizontal loop transmitter. Due to symmetry, the primary field will be vertical directly beneath the center of the loop, with the horizontal component of the primary field increasing when moving away from directly beneath the loop. Multiple angle illumination of the target is achieved by spatially scanning a region above the target. Away from the transmitter loop the signal-to-noise ratio of the signal will decrease significantly, thereby limiting the ability to illuminate the target.

Figure A1 demonstrates how the axial, transverse, and total dipole moment changes as a function of target position and orientation relative to a 1- by 1-m square, horizontal loop transmitter. Directly over a horizontal target (x = 0.0 m), only the transverse component ($L_2(t)$ and $m^2(t)$) contribute to the measured signal. For this case, the transverse dipole (represented by the blue arrow in Figure A1(a), third drawing from the top) is parallel to the induced dipole (represented the red arrow in Figure A1(b), 3rd drawing from the top). The axial component of the dipole is excited when the transmitter is positioned away from the target. The axial and transverse dipoles also contribute to the response. Figure A2 shows the amount of signal due to each polarization at the first time channel of EM-63 data for a horizontal 105-mm projectile at a depth of 1 m. The polarization values used to calculate the response were estimated using data from the USACE-ERDC test stand in Vicksburg, MS. The polarizations at the first time channel are $L_1(t = 0.18 \text{ ms}) = 134.3$ and $L_2(t = 0.18 \text{ ms}) = 78.1$ for the axial and transverse components, respectively.

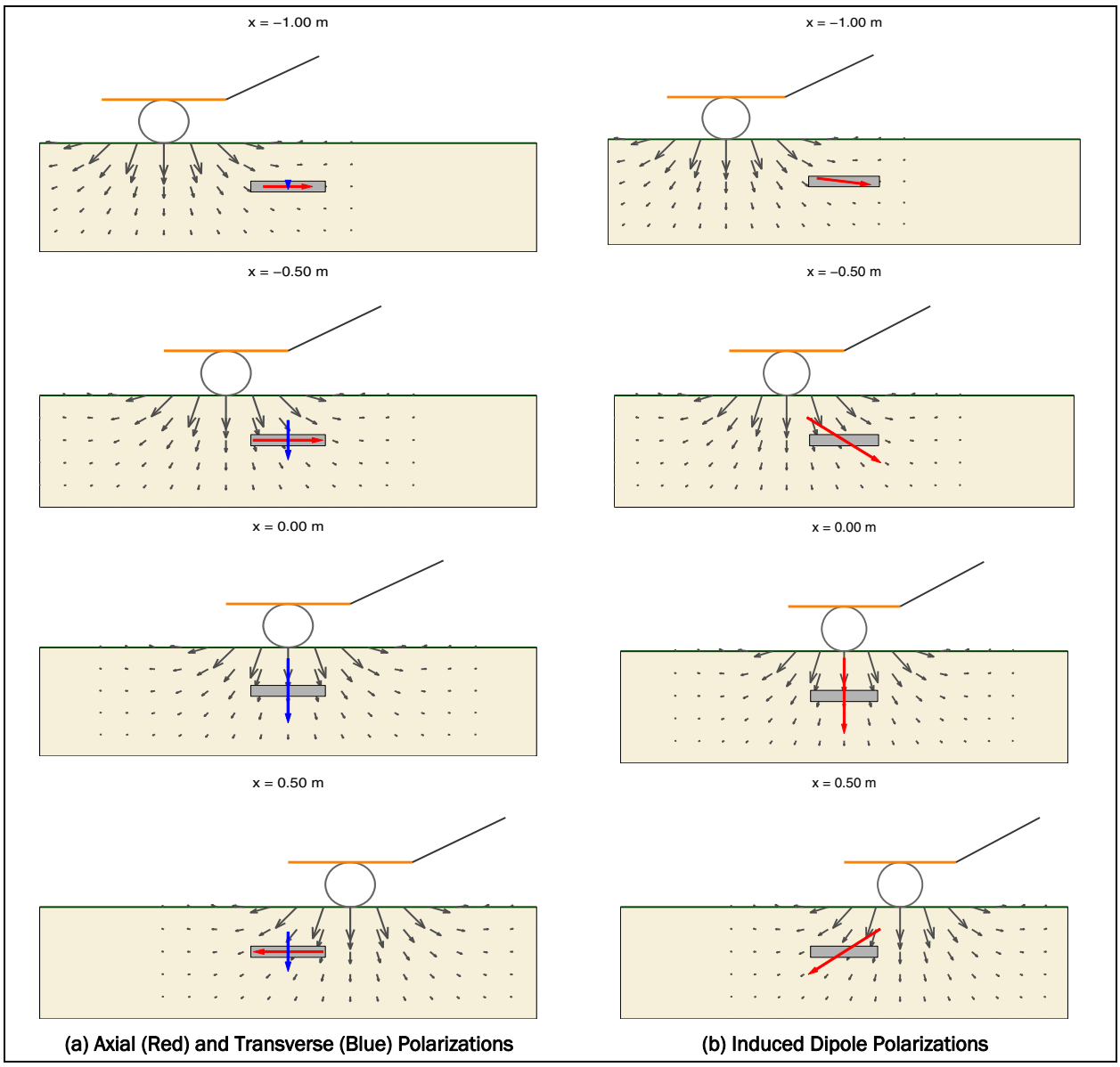

Figure A1. The strength of the induced transverse and axial dipoles for a horizontal, rod-like target. The relative strengths of the polarization values are $L_1/L_2 = 1.72$.

Figure A2(a) shows, in plan view, the forward modeled data with its contributions from the transverse and axial polarizations for the first time channel. The white contour drawn at 2.07 mV represents the estimated standard deviation for noise. The noise statistic was estimated using data from an EM-63 survey carried out on the Sky Research UXO Test Site. Along a line x =0, the projection of the primary field along the axial direction ($\hat{z} \cdot B^P$) is zero, and thus the only contribution to the signal is due to the transverse component. The contribution of axial component makes the anomaly longer along the length of the target.

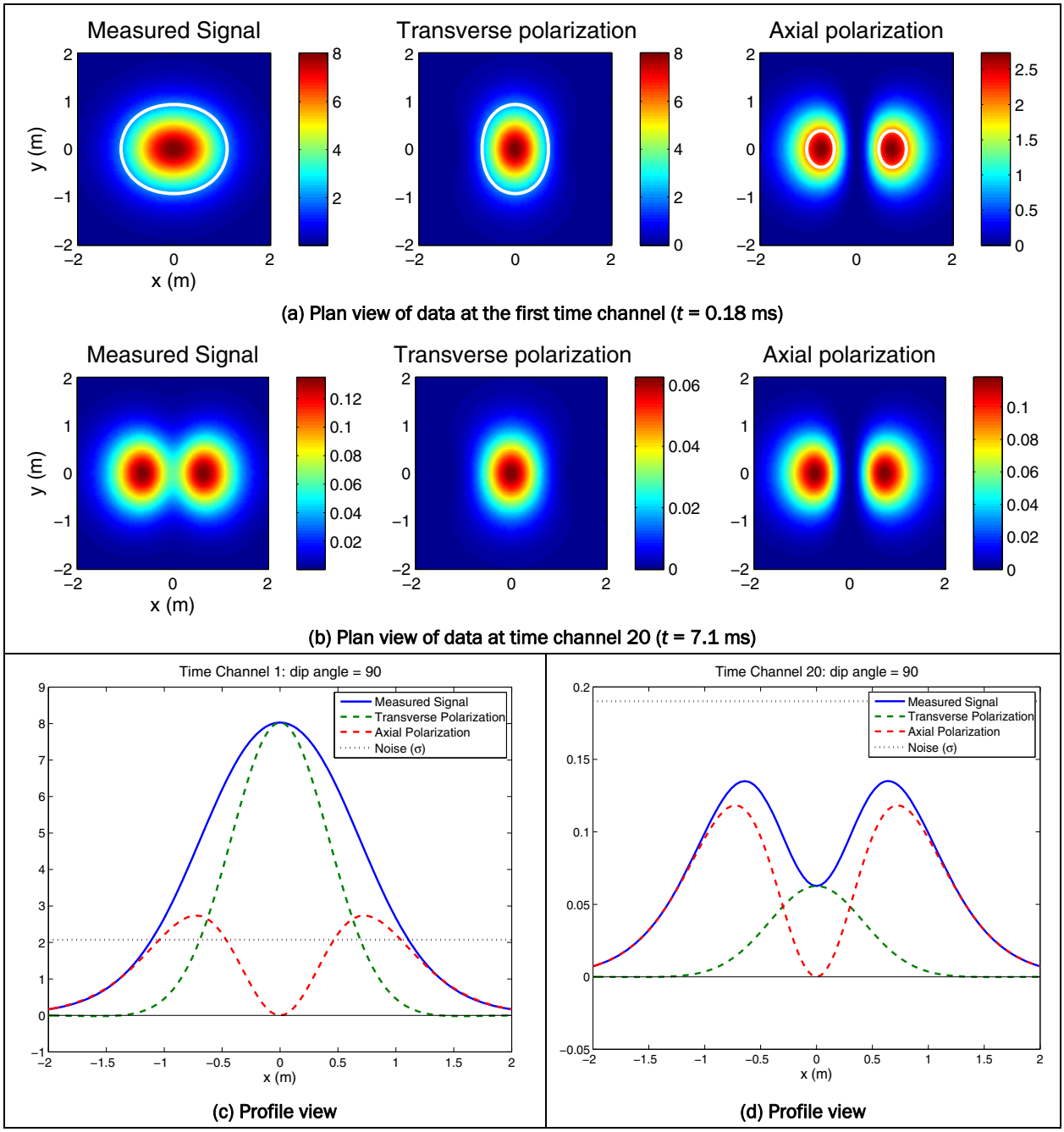

Figure A2. Synthetically generated EM-63 data for a horizontal 105-mm projectile at a depth of 1 m. The polarizations at the first time channel are L_1 (t = 0.18 ms) = 134.3 and L_2 (t = 0.18 ms) =78.1 for the axial and transverse components, respectively. The white contour line in (a) represents the estimated standard deviation for noise, from an EM-63 survey carried out at the Sky Research UXO Test Site. There is no white contour line in (b) because, for t = 7.1 ms, the signal is smaller than the estimated standard deviation of the noise (c), and (d) compare the relative contributions of the axial and transverse polarizations to the measured signal along a line y = 0 m.

For many ordnance, the transverse component will have a smaller time constant than the axial component. In such a case, the late time data will be dominated by the axial component. At later time (Figure A2(b)) the ratio between the axial and transverse component strength is larger ($L_1/L_2(t$ = 0.18 ms) = 1.72, compared to $L_1/L_2(t$ = 7.07 ms) = 5.81/0.61 = 9.52). Therefore, the contribution of the axial component is greater at later times, and the characteristic double-peak anomaly of a horizontal target is observed. Figure A2(c) compares the transverse and axial polarizations along a profile taken at y = 0 m.

The least favorable orientation for resolving both polarizations with a horizontal loop transmitter is for a vertical target (Figure A3). The relationship between the polarization excitations and the transmitter position is the reverse of the horizontal case. The contribution of the transverse excitation to the measured secondary field will be smaller than for the previously considered horizontal target, since (1) the axial polarization will generally be larger than the transverse polarization, and (2) the only way to excite the transverse component is with the cart away from the target, where the signal-to-noise ratio can be small. Figure A5 compares the contributions of the transverse and axial polarizations to the signal from a vertical 105-mm projectile whose center is located at a depth of 1 m below the surface. The transmitter loop is assumed to be 0.4 m above the ground. Indeed, for a deep enough and small enough target, the signal due to the transverse polarization can be less than the noise level of the instrument. For such a case, the ability to identify the target through a data inversion for polarization parameters will be more difficult (Pasion et al., in preparation).

A.2. The similarity between rod and plate responses

Section A1 observed how the response of a target is dependent on the transmitter, receiver, and target geometry. In particular, the response of a rod-like target can be similar to the response of a plate-like target rotated 90 deg (Figure A6). This ambiguity leads to a local minimum at the plate solution when minimizing noisy data from a rod (Pasion et al., in preparation).

To explain why this local minimum might occur, consider the first time channel data from a 105-mm projectile ($L_1(t_1)$ = 134.3 and $L_2(t_1)$ = 78.1). Consider a plate-like target whose polarization parameters at the first time channel are the reverse of the 105-mm projectile, i.e. $L_1(t_1)$ = 78.1and $L_2(t_1)$ = 134.3.

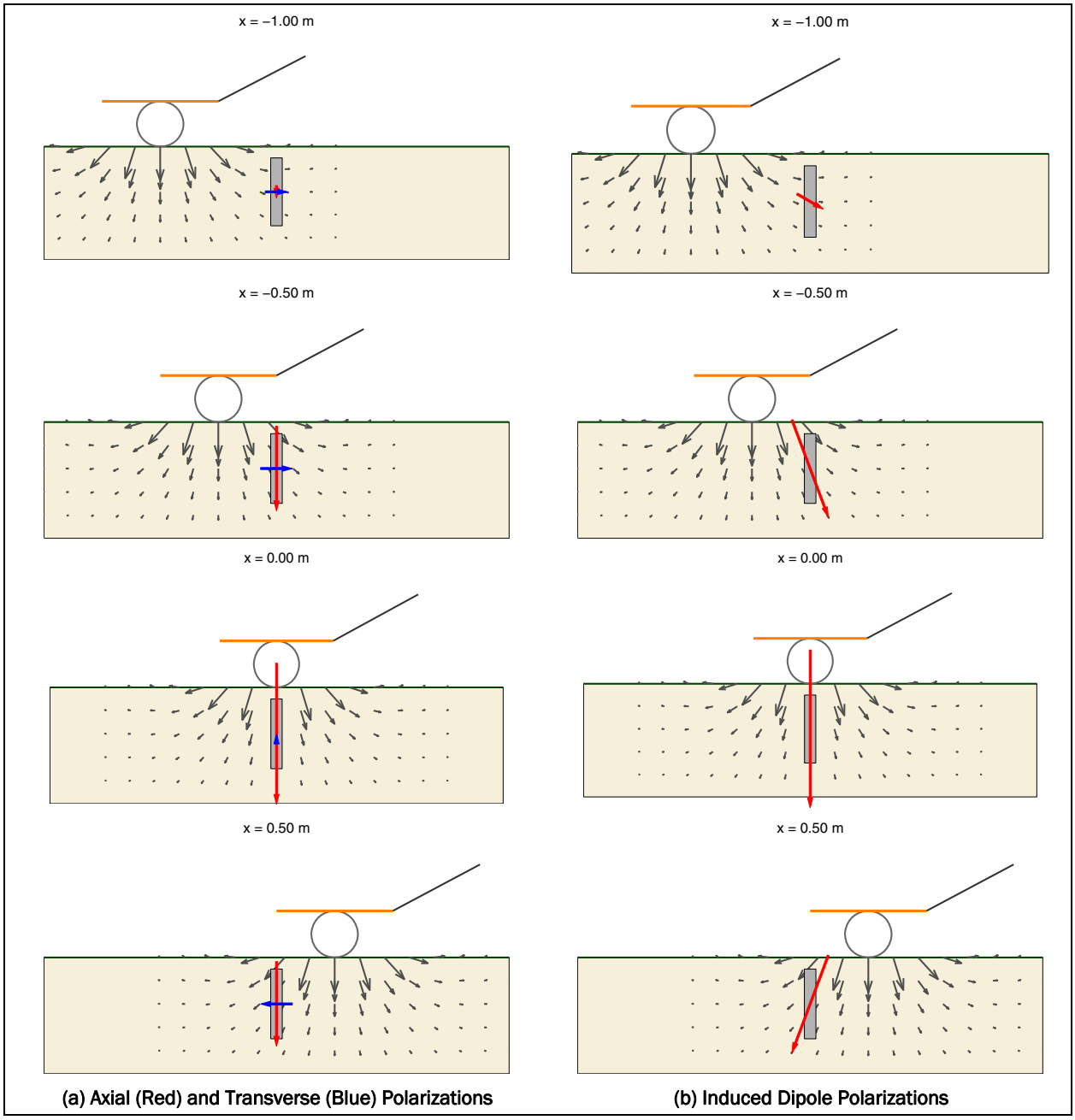

Figure A3. Excitation of a vertical UXO. Relative contributions of the axial (red) and transverse (blue) polarizations are indicated in (a). Excitation of the transverse component occurs when the transmitter loop is positioned away from the target, such that the primary field has a horizontal component. The total induced dipole moment is plotted in (b).

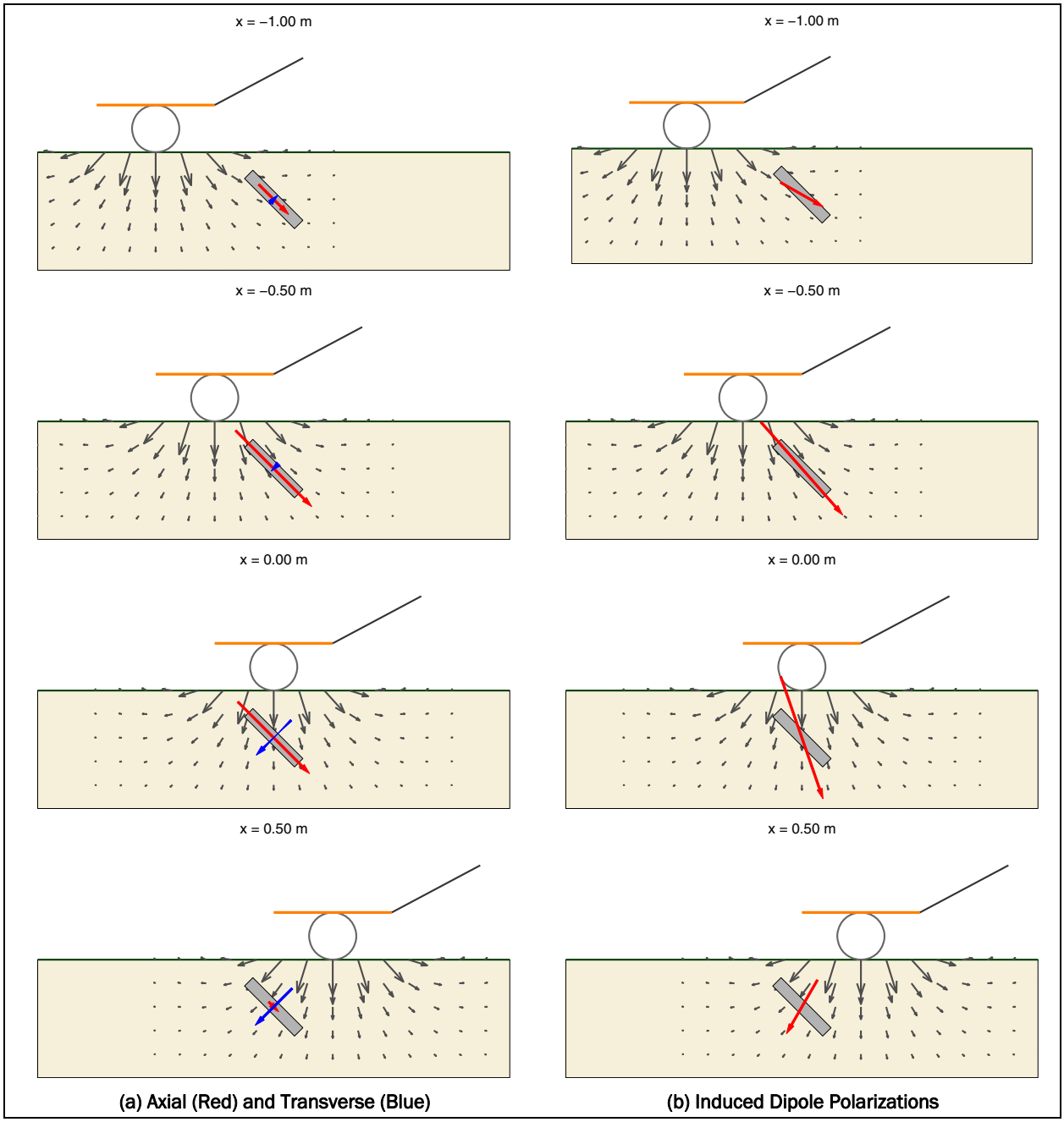

Figure A4. Excitation of a UXO oriented with a 45-deg dip. Relative contributions of the axial (red) and transverse (blue) polarizations are indicated in (a). The total induced dipole moment is plotted in (b).

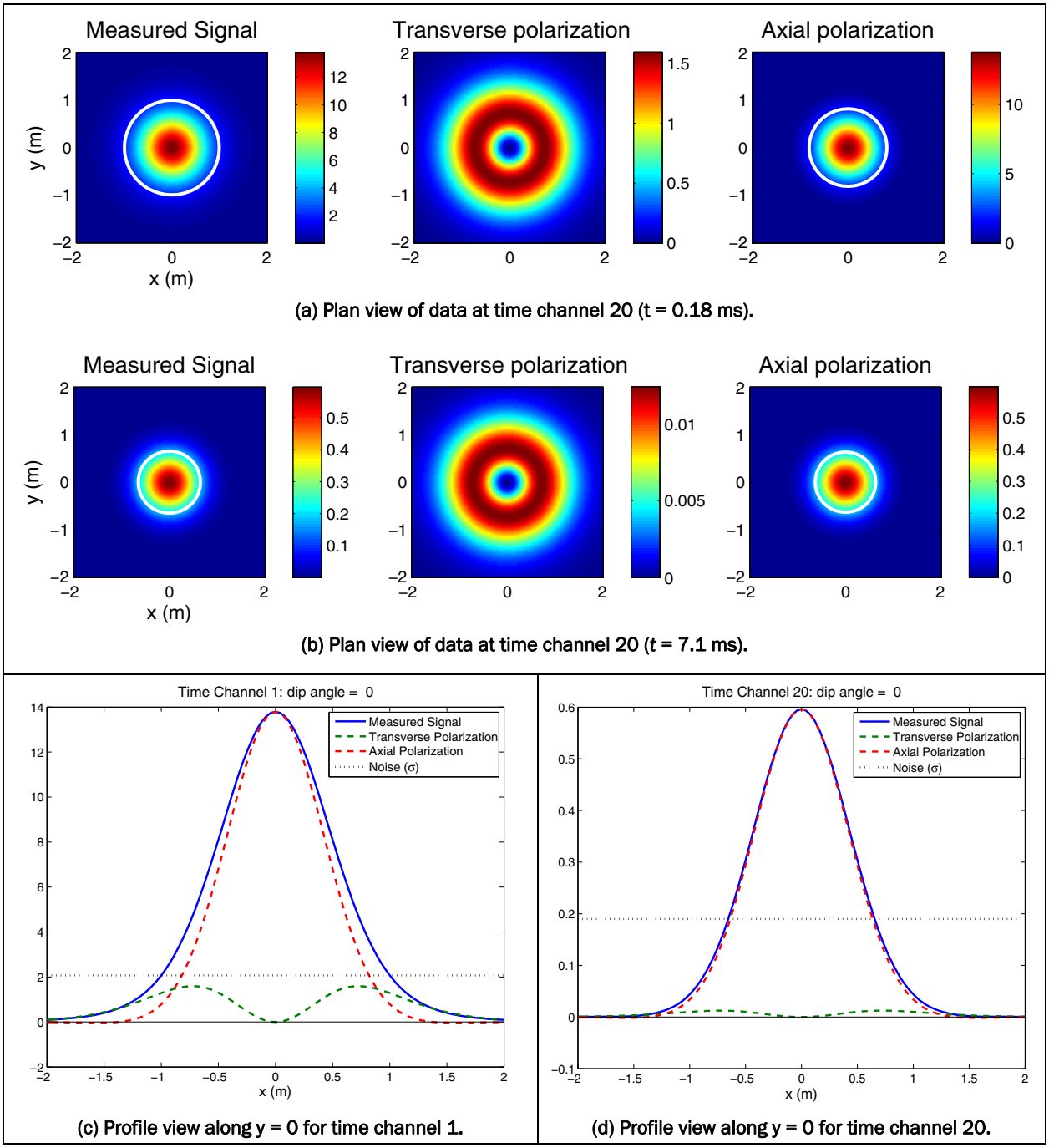

(a) Plan view of data at time channel 20 (t = 0.18 ms).

(b) Plan view of data at time channel 20 (t = 7.1 ms).

(c) Profile view along y = 0 for time channel 1.

(d) Profile view along y = 0 for time channel 20.

Figure A5. Synthetically generated EM-63 data for a vertical 105-mm projectile at a depth of 1 m. The polarizations at the first time channel are L_1 (t = 0.18 ms) = 134.3 and L_2 (t = 0.18 ms) = 78.1 for the axial and transverse components, respectively. The white contour line in (a) represents the estimated standard deviation for noise, from an EM-63 survey carried out at the Sky Research UXO Test Site.

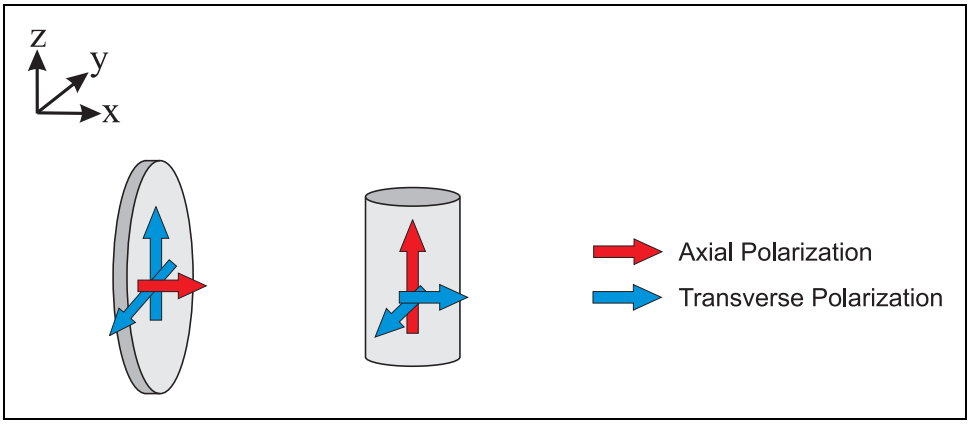

Figure A6. Plate and rod geometry for examples in Figures A7 and A8.

Figure A7 compares the response of the plate and rod oriented as illustrated in Figure A6. The top panels of Figures A7(a) and A7(b) indicate that the responses of the two targets are very similar. The difference between the two responses is plotted in Figure A8. The response of the rod or plate is identical directly above the target, since the primary field is vertical when the sensor is positioned directly above the target and $L_1^{\text{rod}} = L_2^{\text{plate}}$.

Differences in the rod and plate response occur away from directly above the target when horizontal components of the primary field illuminate the target. The signal-to-noise ratio decreases as the sensor moves away from the target, and at some distance from the target, data from a rod will be indistinguishable from the data from a plate-like target.

Figure A9 compares the plate and rod response over data profiles at y = 0 and x = 0. Along a line y = 0 the response of the plate will be identical to the response of the rod. As symmetry suggests, the response of the rod along x = 0 is identical to the rod response along y = 0. The plate response along x = 0 is different, since there is no contribution from its axial component, since the axial component is perpendicular to the primary field along this line. The difference between the rod and plate response along this line is due to a dipole whose strength is proportional to $(y \cdot B^P)\, L_2^{\text{plate}}$.

The above comparison of rod and plate responses is an example of how inadequate signal-to-noise ratio and spatial coverage of the data will lead to ambiguities in the measured data, and thus an inability to robustly recover model parameters through inversion.

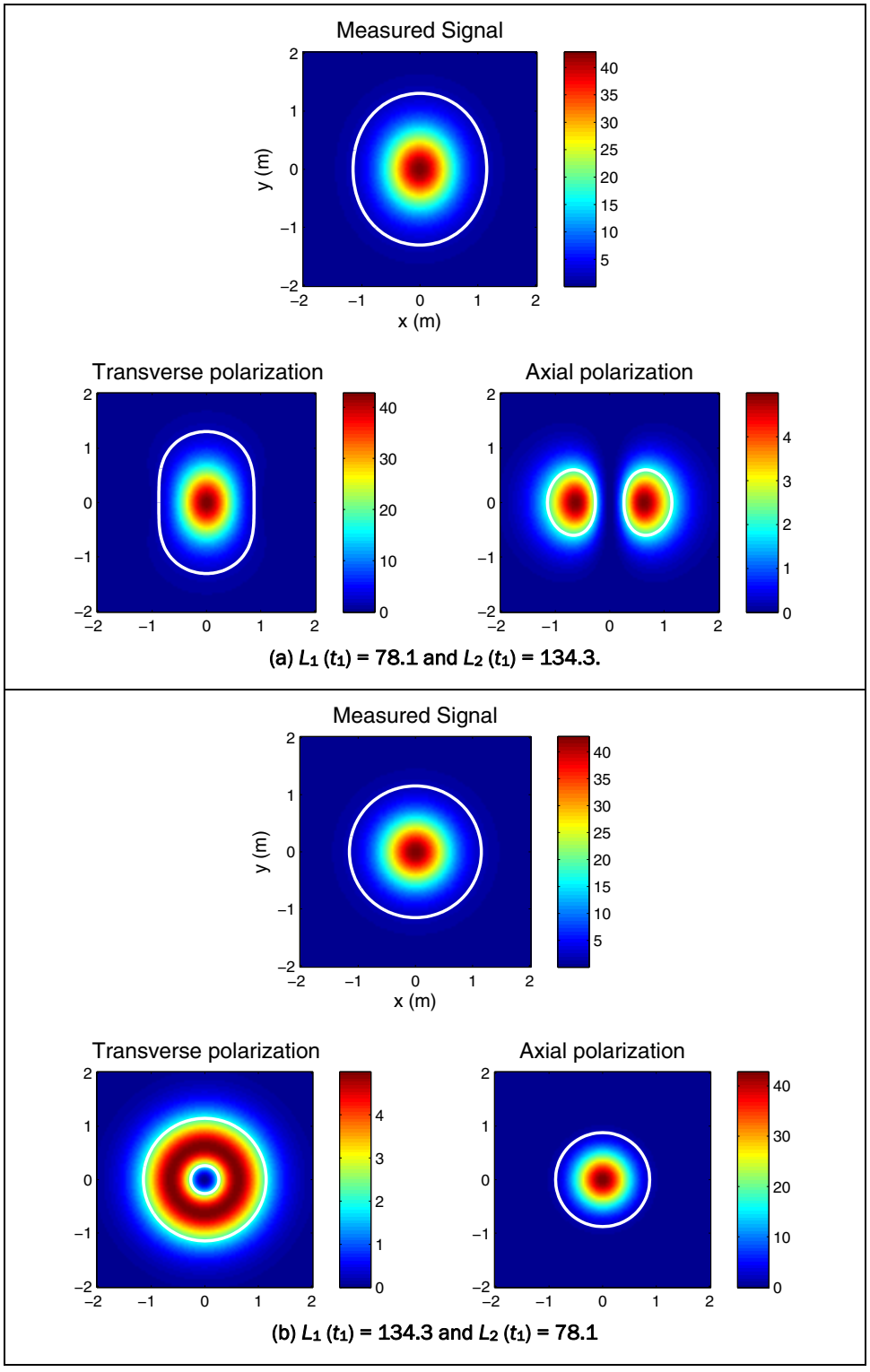

Figure A7. Comparison of the response for (a) a plate-like target whose normal is horizontal and (b) a vertical rod-like target. Since the primary field is predominantly vertical, the response of the plate-like target is mainly due to the polarization induced in the plane of the plate (i.e., the transverse polarization) and the response of the rod is mainly due to the polarization along the rod (i.e. axial polarization). The white contour line indicates the noise level of the EM-63 at the first time channel.

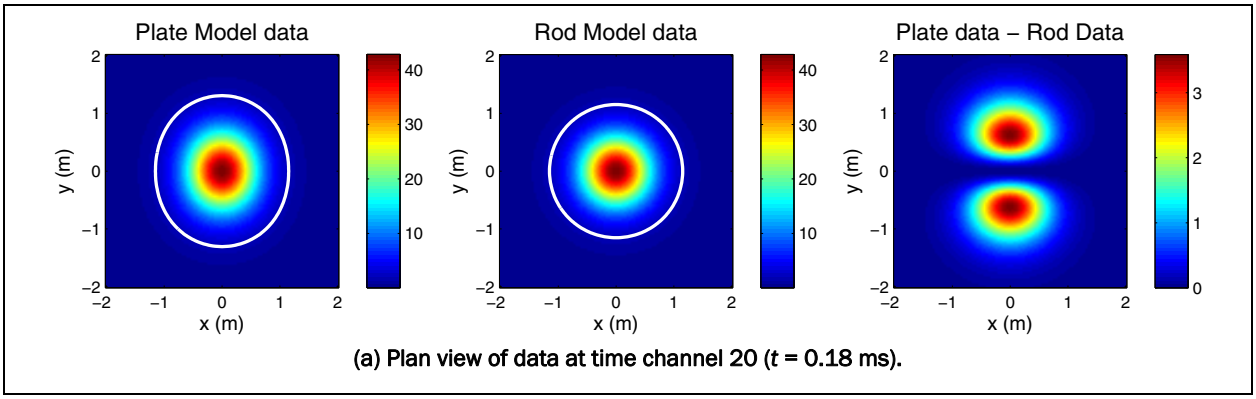

Figure A8. Comparison of the rod and plate data. The right panel shows that the difference between the plate and rod data is of the same order as the standard deviation of the EM-63 noise (σ = 2.07 mV).

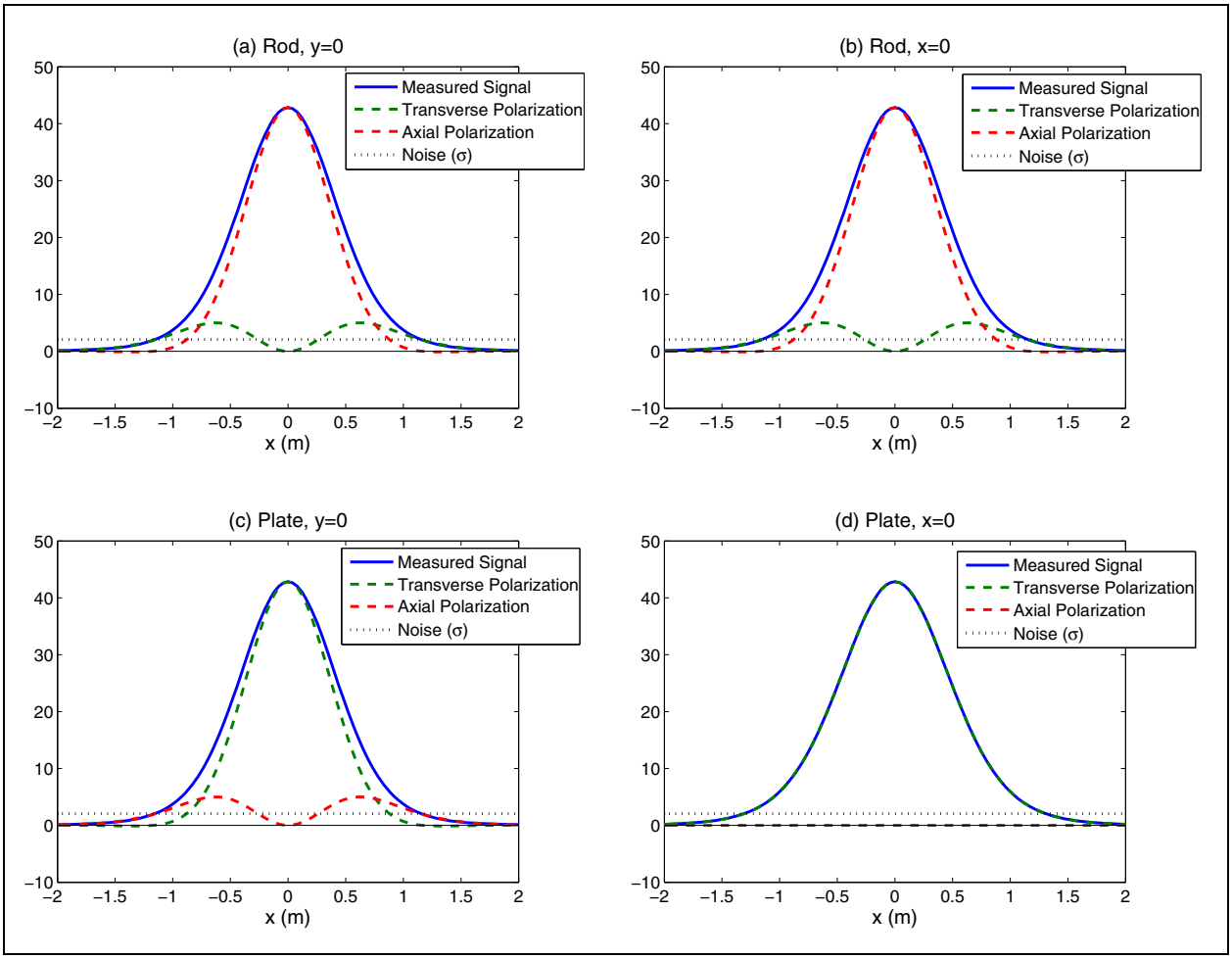

Figure A9. Profiles of the data in Figure A7. The data profile along y = 0 m over either the plate [panel (c)] or rod [panel (c)] is the same. The data profile along x = 0 m is wider over the plate [panels (b)] than the rod [panel (d)].

REPORT DOCUMENTATION PAGE

Form Approved
OMB No. 0704-0188

1. REPORT DATE *(DD-MM-YYYY)*	2. REPORT TYPE	3. DATES COVERED *(From - To)*
September 2008	Report 6 of 9	

4. TITLE AND SUBTITLE

UXO Characterization: Comparing Cued Surveying to Standard Detection and Discrimination Approaches: Report 6 of 9 – Advanced Electromagnetic and Magnetic Methods for Discrimination of Unexploded Ordnance

5a. CONTRACT NUMBER
W912HZ-04-C-0039

5b. GRANT NUMBER

5c. PROGRAM ELEMENT NUMBER

6. AUTHOR(S)

Stephen D. Billings, Leonard R. Pasion, Nicolas Lhomme, and Lin Ping Song

5d. PROJECT NUMBER

5e. TASK NUMBER

5f. WORK UNIT NUMBER

7. PERFORMING ORGANIZATION NAME(S) AND ADDRESS(ES)

Sky Research, Inc.
445 Dead Indian Memorial Road
Ashland, OR 97520

8. PERFORMING ORGANIZATION REPORT NUMBER

ERDC/EL TR-08-37

9. SPONSORING / MONITORING AGENCY NAME(S) AND ADDRESS(ES)

Headquarters, U.S. Army Corps of Engineers
Washington, DC 20314-1000;
U.S. Army Engineer Research and Development Center
Environmental Laboratory
3909 Halls Ferry Road, Vicksburg, MS 39180-6199

10. SPONSOR/MONITOR'S ACRONYM(S)

11. SPONSOR/MONITOR'S REPORT NUMBER(S)

12. DISTRIBUTION / AVAILABILITY STATEMENT

Approved for public release; distribution is unlimited.

13. SUPPLEMENTARY NOTES

14. ABSTRACT

The magnetic and electromagnetic induction models and inversion strategies that are used to discriminate hazardous UXO from non-hazardous shrapnel and scrap metal are described. Discrimination methods typically proceed by first recovering a set of parameters that specify a physics-based model of the object being interrogated. For EMI, a polarizability model is commonly used. For magnetics, the physics-based model is generally a static magnetic dipole. Once the parameters are recovered by inversion, a subset of the parameters is used as feature vectors to guide a statistical or rule-based classifier. The dipole-based inversion and classification scheme is described and a number of variations are considered, including: 1) Dipole-based template matching whereby the object's identity is selected as the best fitting polarization model from a predefined library of objects; 2) SEA, where the dipole model is replaced with a physically complete forward-modeling scheme. SEA is also a template-matching approach; and 3) SMC, where the dipole model is replaced by a fictitious charge distribution on a circle or ellipse that encloses the UXO or clutter object. The total SMC is then used as a feature vector in a statistical or rule-based classification scheme.

15. SUBJECT TERMS

EMI sensors
Frequency-domain electromagnetic induction (FEM)
Ground penetrating radar
Time-domain electromagnetic induction (TEM)
Total-field magnetics
Unexploded ordnance (UXO)
UXO discrimination

16. SECURITY CLASSIFICATION OF:			17. LIMITATION OF ABSTRACT	18. NUMBER OF PAGES	19a. NAME OF RESPONSIBLE PERSON
a. REPORT	b. ABSTRACT	c. THIS PAGE			19b. TELEPHONE NUMBER *(include area code)*
UNCLASSIFIED	UNCLASSIFIED	UNCLASSIFIED		56	